POLITECNICO
MILANO 1863

SCUOLA DI INGEGNERIA INDUSTRIALE
E DELL'INFORMAZIONE

Station-Keeping Strategies for Libration Point Orbits with Applications to the LUMIO Mission

Tesi di Laurea Magistrale in
Space Engineering - Ingegneria Aerospaziale

Author: **Filippo Zanellati**

Student ID: 971089
Advisor: Prof. Francesco Topputo
Co-advisors: Carmine Giordano, Carmine Buonagura
Academic Year: 2021-22

"It was Gravity!"
Murph

Abstract

Orbits about libration points offer unique possibilities for space missions, allowing configurations that are fixed with respect to two primary bodies. However, the major drawback associated with those trajectories is their inherent instability. Due to the presence of the unstable manifold, even a small perturbation can cause a spacecraft to completely diverge from its reference path. The design of a suitable orbit maintenance strategy is thus vital for the success of the missions.

The focus of this work is the station-keeping problem. The analysis is carried out using three different methods: target point, Floquet mode, and short term approach. The algorithms are then applied to the case study of LUMIO mission, with the goals of improving its station-keeping performance, and exploring different solutions.

The simulations are executed in a computational environment, which involves the high fidelity roto-pulsating restricted n-body problem, to propagate the motion of the spacecraft, and various operational errors, to estimate the station-keeping cost with little approximation. The results are obtained with a Monte Carlo analysis, to ensure their statistical significance. Finally, the strategies are compared and contrasted, and validated against literature sources.

Keywords: Halo Orbit, Station-Keeping, Target Point Approach, Floquet Modes, Short Term Approach.

Abstract in lingua italiana

Le orbite nell'intorno dei punti di Lagrange offrono possibilità uniche per le missioni spaziali, consentendo configurazioni stazionarie nei confronti di due corpi primari. Tuttavia, il principale svantaggio associato a queste traiettorie è la loro instabilità. Per questo motivo, anche piccole perturbazioni possono causare una rapida divergenza del satellite dalla sua traiettoria di riferimento. Il progetto di una strategia di mantenimento dell'orbita è di conseguenza vitale per il successo delle missioni.

Questo lavoro di ricerca è focalizzato sul problema dello station-keeping. L'analisi viene svolta usando tre strategie differenti: il target point, il Floquet mode, e lo short term approach. Questi algoritmi vengono successivamente applicati al caso studio della missione LUMIO, con l'obiettivo di migliorare le sue performance, e di esplorare nuove soluzioni.

Le simulazioni vengono svolte in un ambiente computazionale, che include un modello ad alta fedeltà nel sistema roto-pulsante per integrare le equazioni di moto, e degli errori operativi per approssimare le vere condizioni di missione. I risultati sono ottenuti con un'analisi Monte Carlo, per assicurare significatività statistica. Infine, le strategie sono confrontate l'una con l'altra, e validate utilizzando risultati della letteratura scientifica.

Parole chiave: Orbita Halo, Station-Keeping, Target Point Approach, Modi di Floquet, Short Term Approach.

Contents

1 | Introduction

CubeSats are small artificial satellites, composed of units of standardized dimensions, equal to $10 \times 10 \times 10$ cm, or 1U. The interest in using this class of spacecraft for space missions has been rising in recent times, owing to their lower cost, that allows more players to fund their own ones [33]. Furthermore, CubeSats are more scalable, can be built using "off the shelf" components, and, due to their small volume, can be launched with greater ease and less budget.

Almost all of these satellites are launched into Earth-centered orbits, though other types of trajectories will undoubtedly be investigated for future missions. Studies on the Moon, for example, could use libration point orbits to perform their activity in a fixed configuration with respect to both the Moon and the Earth. To design such missions, one has to consider the circular restricted three-body problem (CR3BP), a dynamical model that considers the gravity of two different bodies.

One major downside associated with CubeSats is their weak, or worse absent, propulsion system. This fact is usually compensated by the choice of their trajectories, that require little to no attention to orbit maintenance. However, when designing a mission about a libration point orbit, the station-keeping problem, defined as the problem of keeping the spacecraft near its reference trajectory, becomes central, because those trajectories may be unstable. These two facts, coupled together, create the need for a deeper investigation regarding the orbit maintenance strategies employed for such missions. Hence the main motivations and the goals of this work, which are explained hereafter, and are formulated on the basis of the previous considerations.

1.1. Motivations and Goals

The circular restricted three-body problem, due to its dynamics, provides special configurations for use in space applications. The presence of equilibrium points and periodic orbits enables missions with spacecrafts that are fixed with respect to two primary bodies. In addition, the stable and unstable manifolds can be exploited through ballistic captures,

a type of transfer that requires minimal fuel consumption. Those considerations, combined together, explain why the interest in libration point missions is consistently rising within the scientific community.

When designing a mission for a lagrangian point, the orbit maintenance cost may take up a substantial fraction of the fuel budget, because some of these trajectories are unstable. In addition to the instability of the orbit, it must be considered that a spacecraft is not perfectly injected onto the trajectory, and that the position of the spacecraft is known with some error. All of these deviations from the nominal path are unavoidable, and must be corrected with a suitable station-keeping strategy.

As a result, the primary goal of this work is to implement a method that solves the station-keeping problem for a libration point orbit. In addition to the inherent instability of the trajectory, the algorithm shall be able to model and compensate for the operational errors made during the mission. The investigation is carried out on a halo orbit about the second lagrangian point in the Earth-Moon system, by implementing multiple strategies, selected through a trade-off, that are subsequently compared and contrasted.

To produce more realistic and useful results, the parameters of the simulations are set considering a case study, which is LUMIO. It is a CubeSat mission, planned by the European Space Agency, for an orbit which coincides with the scope of this work. The station-keeping strategies are thus implemented while taking into account the parameters used in the design of LUMIO, as well as its reference trajectory. With the design of the mission already under development, a baseline orbit maintenance strategy has already been selected. The goal of this work is to improve the baseline method, by tuning its parameters, and to experiment with new strategies, to see if they can outperform the one that has already been tested.

1.2. Literature Review

A current and reliable analysis of the dynamics of the circular restricted three-body problem is offered by Szebehely [29]. Leonhard Euler and Giuseppe Lodovico Lagrangia, in the 18-th century, demonstrated the existence of five equilibrium points, and Jacobi computed an integral of motion [29]. In relation to the model, Markeev [23] examined the stability of those equilibrium points, and Moser [24] demonstrated that there are families of periodic orbits revolving around them. Doedel et al. [10] classified these trajectories into different categories.

The roto-pulsating restricted n-body problem (RPRnBP) represents a more accurate de-

scription of reality. Gomez et al. [18] computed the dynamical substitutes for libration points, and demonstrated how to continue the invariant manifolds in increasingly complex models. In addition, Dei Tos and Topputo [8] described a method concerning how to produce quasi-periodic orbits in the RPRnBP, that are similar to libration point orbits in the CR3BP.

The investigation on how to control a spacecraft on libration point orbits began in the sixties, when Farquahr [11] proposed station-keeping techniques based on feedback control laws. The first work regarding halo orbits about the point L2 in the Earth-Moon system is dated 1974, and belongs to Breakwell et al [3]. Although it was in the Sun-Earth system, the ISEE-3 mission [12] marked the beginning of the use of libration point orbits for mission-related purposes. Impulsive maneuvers allowed the spacecraft to remain in the vicinity of the desired orbit. The first mission on a halo orbit about the second lagrangian point in the Earth-Moon system, which is the one of interest in this investigation, was Genesis [22], which was launched in 2001.

Thanks to the growing interest in libration point missions, various station-keeping strategies have been investigated. Floquet mode approach, first cited by Wiesel and Shelton [34], and better developed by Simò et al. [16], computes maneuvers that cancel the unstable character of the orbit. Another strategy is target point approach, first presented by Howell and Pernika [20], that computes maneuvers by minimizing a weighted cost function. The two methods cited above were compared by Keeter [19], on a halo orbit in the Sun-Earth system.

Other targeting strategies were investigated by Pavlak [25], Folta et al. [14], and Pavlak and Howell [26], all in the framework of the ARTEMIS mission. Those strategies make use of the multiple-shooting method, to compute fuel-optimal maneuvers that match user imposed constraints, to continue the orbit or to meet end of life conditions.

Lian et al. [21] exploited sliding mode control to stabilize a spacecraft in a libration point orbit, using the linearized and discretized equations of motion, to keep the state near a sliding surface. Finally, Bai and Junkins [2] applied the modified Chebishev-Picard iteration method to stabilize a halo orbit, stating the station-keeping problem as a two-point boundary-value problem.

A review of all the libration point missions and strategies was performed by Shirobokov et al [28], and it is summarized in Table 1.1.

Table 1.1: Review of Previous Libration Point Missions [28]

Mission	Launch Date	Orbit	A_y, $A_z[10^3\text{km}]$	Δv[m/s/y]
ISEE-3	12/08/1978	Halo (SE L_1)	666.67, 120.0	8.5
Wind	01/11/1994	Quasi-Halo (SE L_1)	640.0, 170.0	1.0
SOHO	02/12/1995	Halo (SE L_1)	666.67, 120.0	2.4
ACE	25/08/1997	Lissajous (SE L_1)	264.0, 157.41	1.0
WMAP	30/06/2001	Lissajous (SE L_2)	264.0, 264.0	1.2
Genesis	08/08/2001	Quasi-Halo (SE L_1)	800.0, 450.0	9.0
		Quasi-Halo (EM L_2)	63.52, 35.20	7.39
ARTEMIS	17/02/2007	Quasi-Halo (EM L_1)	58.82, 2.39	5.28
		Quasi-Halo (EM L_1)	67.71, 4.68	5.09
Herschel	14/05/2009	Halo (SE L_2)	700.0, 400.0	1.0
Planck	14/05/2009	Lissajous (SE L_2)	300.0, 300.0	1.0
Chang'e 2	01/10/2010	Lissajous (SE L_2)	918.0, 400.0	$\sim$
Gaia	19/12/2013	Lissajous (SE L_2)	350.0, 100.0	2.0
Chang'e 5-T1	23/10/2014	Lissajous (EM L_2)	40.0, 35.0	$\sim$
DSCOVR	11/02/2015	Lissajous (SE L_1)	264.1, 157.4	$\sim$
LISA Pathfinder	03/12/2015	Quasi-Halo (SE L_1)	800.0, 600.0	1.8

1.3. Research Question

The research question is formulated mainly considering the objectives of the work. The first interest is to study and implement the station-keeping of a libration point orbit. However, considering that the case study of the work is LUMIO mission, the strategies implemented can also be compared and contrasted with the baseline of the mission. Finally, the best outcome would be to improve the baseline station-keeping method, thus lowering the mission's fuel budget. Those considerations lead to the formulation of the following research question:

To what extent is it possible to improve the station-keeping of a mission at the Earth-Moon second lagrangian point?

1.4. Organization of the Work

The work is organized into different chapters, which are presented hereafter:

Dynamical Models. Chapter 2 serves the purpose of introducing the equations used in this work to integrate the dynamics of the spacecraft. The circular restricted three-body problem is first explained, which is the framework in which libration point

orbits are constructed. After that, the roto-pulsating n-body problem is described, which is needed to find results with higher fidelity for the mission.

Station-Keeping Strategies. Various examples of station-keeping techniques are explained in Chapter 3. The strategies are divided in methods based on dynamical effects, and of general control theory. The Chapter ends with a trade-off between the techniques, to choose the most interesting ones to implement for this research.

Target Point Approach. Chapter 4 starts with the definition of the station-keeping problem. It describes the operational errors and the Monte Carlo simulation, which are common features of all the strategies analyzed in this work. As the title suggests, the main topic of the Chapter is the description of the target point approach, which is the first method implemented in this work.

Floquet Mode Approach. The theoretical framework of Floquet modes is provided in the beginning of Chapter 5. Then, two types of controller are designed, which aim at cancelling the unstable component of the spacecraft's motion. The Chapter ends with the station-keeping algorithm, which is very similar to the one of target point, and the objectives of the analysis.

Short Term Approach. Short term approach is the last method to be implemented in this thesis and is presented in Chapter 6. The first topic to be touched is the simple-shooting method, which is used to compute the maneuvers of this strategy. After that, the algorithm and the objectives are presented.

Results. After the theoretical framework given by the previous Chapters, Chapter 7 presents the results obtained with the implementation of the station-keeping strategies. The first section gives a brief outline of LUMIO mission, and presents the parameters used for the simulations. The latter three sections show the results of the three methods chosen during the trade-off.

Conclusions. The last chapter, which is Chapter 8, sums up the work and gives some final thoughts about the results. It finally proposes future ways to improve the results obtained.

2 | Dynamical Models

The motion of any massive body $i = 1, ..., n$, in a gravitational environment, is, in the most general case, governed by Newton's universal law of gravitation

$$\boldsymbol{F}_{ji} = -G \sum_{\substack{j=1 \\ j \neq i}}^{n} \frac{m_i m_j}{r_{ji}^3} \boldsymbol{r}_{ji}, \qquad i = 1, \ldots, n. \tag{2.1}$$

The vector $\boldsymbol{r_{ji}}$ is the relative position of the i-th body with respect to the j-th body. Using the same notation, $\boldsymbol{F_{ji}}$ is the force exerted on the i-th body by the j-th body.

By remembering Newton's second law of dynamics, it is possible to write the equations of motion of the system

$$m_i \ddot{\boldsymbol{r}}_i = -G \sum_{\substack{j=1 \\ j \neq i}}^{n} \frac{m_i m_j}{r_{ji}^3} \boldsymbol{r}_{ji}, \qquad i = 1, \ldots, n. \tag{2.2}$$

Systems with $n > 2$ don't have an analytical solution, neither a formulation which is time independent. For this reason, to understand the behaviour of a system, it is necessary to make simplifying assumptions to formulate a time invariant model. In the case of this work, which is focused on a Earth–Moon libration point orbit, a time independent model, which considers only the gravitational influence of the Earth and the Moon, is suitable as a first approximation. This model is the circular restricted three-body problem.

2.1. The Circular Restricted Three-Body Problem

2.1.1. Equations of Motion

The equations of motion of three massive bodies under mutual gravitational attraction may be written as Equation (2.2) with $i = 1, 2, 3$. However, the CR3BP requires some additional assumptions.

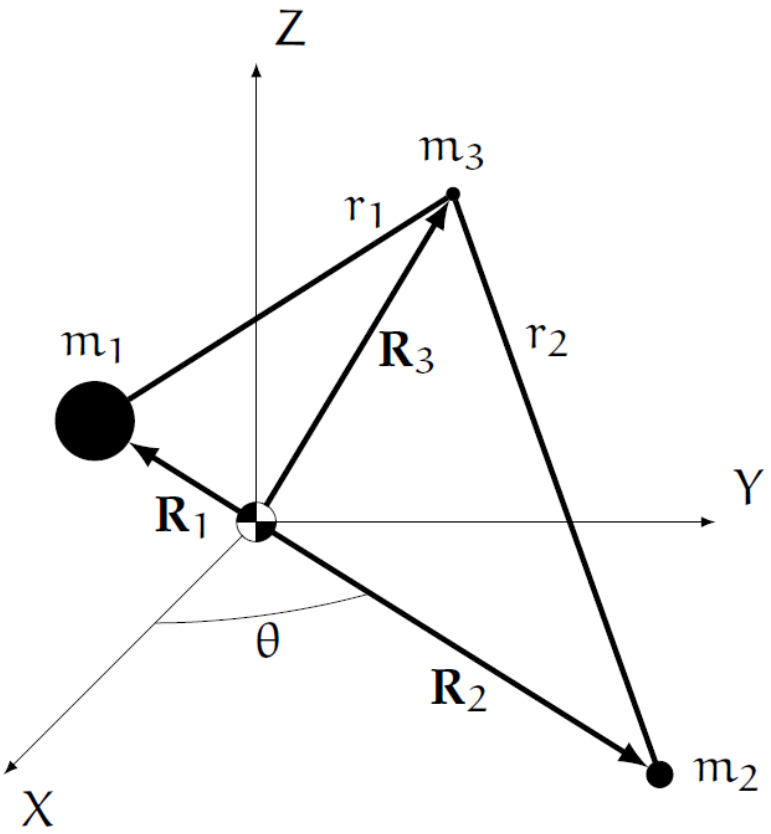

Figure 2.1: Geometry of the Circular Restricted Three-Body Problem [6]

The restricted hypothesis imposes the mass of the third body (the spacecraft), to be much smaller than the mass of the two primaries (the Earth and the Moon), i.e $m_3 << m_2 < m_1$. Physically, this implies Keplerian motion of the two primaries with respect to the system's center of mass, with no influence from the third mass. The center of gravity of the system, which coincides with the one of m_1 and m_2, is used as the origin of the frame of reference.

Additionally, the circular hypothesis requires circular motion of the two primaries, bounded to the (X, Y) plane, with constant angular speed ω_2. For reference, the geometry of the CR3BP can be seen in Figure 2.1.

Consequently, the equations of motion can be written as [6]

$$\ddot{X} = -G\left(m_1\frac{X + a\cos\theta}{r_1^3} + m_2\frac{X - b\cos\theta}{r_2^3}\right), \tag{2.3a}$$

$$\ddot{Y} = -G\left(m_1\frac{Y + a\sin\theta}{r_1^3} + m_2\frac{Y - b\sin\theta}{r_2^3}\right), \tag{2.3b}$$

$$\ddot{Z} = -G\left(m_1\frac{Z}{r_1^3} + m_2\frac{Z}{r_2^3}\right), \tag{2.3c}$$

where r_1 and r_2 are the radii of the third body with respect to m_1 and m_2, a and b are the radii of the two primaries with respect to the system's center of gravity, and θ is the angle between the X axis and the direction of m_1 and m_2.

It can be convenient to rewrite the equations of motion in the synodic frame of reference $[\hat{x}, \hat{y}, \hat{z}]$, which is rotating in such a way to maintain the primaries at fixed positions on the $\hat{x}$ axis. To do so, it is necessary to rotate the previous equations of motion, which were written in the sidereal reference frame. The rotation matrix reads

$$R = \begin{bmatrix} \cos\theta & -\sin\theta & 0 \\ \sin\theta & \cos\theta & 0 \\ 0 & 0 & 1 \end{bmatrix}. \tag{2.4}$$

By defining $\boldsymbol{\rho}$ such that $\boldsymbol{r} = R\boldsymbol{\rho}$, and ω_2 such that $\theta = \omega_2 t$, the equations of motion, in matrix form, become

$$\ddot{\hat{\boldsymbol{\rho}}} = -2R^T\dot{R}\dot{\hat{\boldsymbol{\rho}}} - R^T\ddot{R}\hat{\boldsymbol{\rho}} - G\left(m_1\frac{\hat{\boldsymbol{\rho}} - \hat{\boldsymbol{\rho}}_1}{||\hat{\boldsymbol{\rho}} - \hat{\boldsymbol{\rho}}_1||^3} + m_2\frac{\hat{\boldsymbol{\rho}} - \hat{\boldsymbol{\rho}}_2}{||\hat{\boldsymbol{\rho}} - \hat{\boldsymbol{\rho}}_2||^3}\right). \tag{2.5}$$

Equation (2.5) can be simplified even more by introducing dimensionless variables, constructed such that the distance between the primaries, the angular rate and the sum of their masses have unitary values. The values are [29]

$$\boldsymbol{\rho} = \frac{\hat{\boldsymbol{\rho}}}{a+b}, \qquad \tau = \omega_2 t, \qquad \mu = \frac{m_2}{m_1 + m_2}. \tag{2.6}$$

With this adimensionalisation, the positions of the primaries become $(-\mu, 0, 0)$ and $(1-\mu, 0, 0)$, respectively.

Finally, the dimensionless equations of motion can be written as [28]

$$\ddot{x} - 2\dot{y} = \Omega^{(3)}_{/x}, \tag{2.7a}$$
$$\ddot{y} + 2\dot{x} = \Omega^{(3)}_{/y}, \tag{2.7b}$$
$$\ddot{z} = \Omega^{(3)}_{/z}, \tag{2.7c}$$

where $\Omega^{(3)}$ is the pseudo-potential of the CR3BP, defined as

$$\Omega^{(3)} = \frac{1}{2}\left(x^2 + y^2\right) + \frac{1-\mu}{r_1} + \frac{\mu}{r_2} + \frac{1}{2}\mu(1-\mu). \tag{2.8}$$

The equations of motion written in this form, which is autonomous, posses a first integral of motion, called the Jacobi integral. Its expression is:

$$J = 2\Omega^{(3)} - \left(\dot{x}^2 + \dot{y}^2 + \dot{z}^2\right). \tag{2.9}$$

2.1.2. Lagrangian Points

The CR3BP possesses five equilibrium points, located where the spatial derivatives of the Jacobi integral are null. The condition reads

$$\Omega^{(3)}_{/x} = x - \frac{(1-\mu)(x+\mu)}{\rho_1^3} - \frac{\mu(x-1+\mu)}{\rho_2^3} = 0, \tag{2.10a}$$

$$\Omega^{(3)}_{/y} = y\left(1 - \frac{1-\mu}{\rho_1^3} + \frac{\mu}{\rho_2^3}\right) = 0, \tag{2.10b}$$

$$\Omega^{(3)}_{/z} = -z\left(\frac{1-\mu}{\rho_1^3} + \frac{\mu}{\rho_2^3}\right) = 0. \tag{2.10c}$$

From the third equation it is trivial that the Lagrangian points lie on the (x, y) plane.

The second conditions has $\rho_1 = \rho_2 = 1$ as a solution. It means that two of the equilibrium points form equilateral triangles with the primaries. These equilibrium points are called L_4 and L_5, and their coordinates are respectively:

$$L_4 : \left(\frac{1}{2} - \mu, \frac{\sqrt{3}}{2}, 0\right), \qquad L_5 : \left(\frac{1}{2} - \mu, -\frac{\sqrt{3}}{2}, 0\right). \tag{2.11}$$

The solution of the first condition is, on the other hand, more difficult, and requires a numerical technique. The results are three equilibrium points, on the x axis, called collinear libration points. Their abscissas, in the Earth Moon system, are [7]:

$$L_1 : 0.83691513, \qquad L_2 : 1.15568226, \qquad L_3 : -1.005062645. \tag{2.12}$$

It is visible how L_1 is between the two bodies, L_2 is behind the lower mass body, and L_3 is behind the higher mass body.

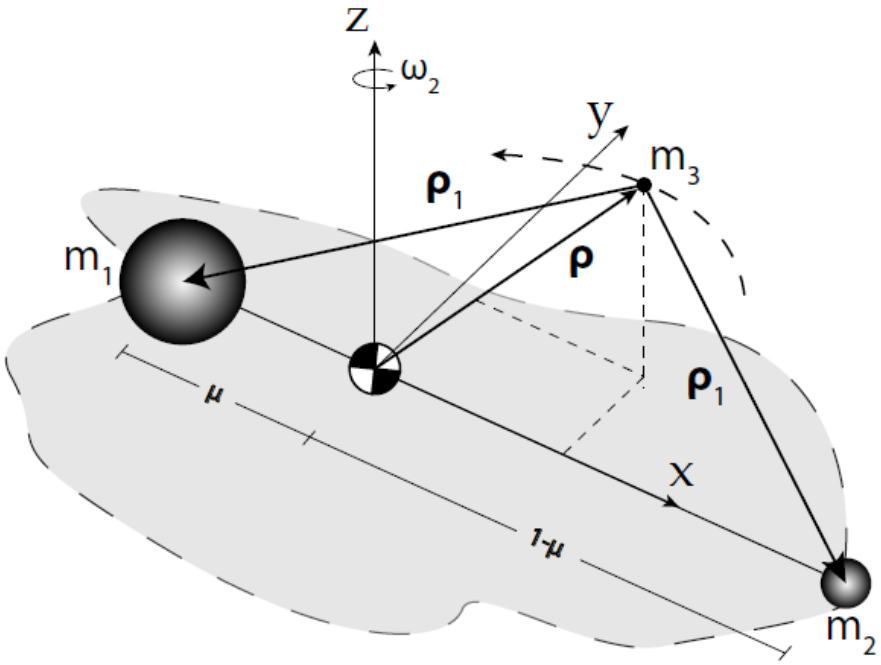

Figure 2.2: Geometry of the Roto-Pulsating Frame [7]

2.2. The Roto-Pulsating Restricted n-Body Problem

As the CR3BP is used as a base approximation to understand the physics of the system, a more detailed model is required to produce a more accurate analysis. This model is the roto-pulsating restricted n-body problem (RPRnBP), which is the one used in the simulations of this work. In this model, the motion of the two primaries is elliptical and no longer circular. The RPRnBP considers additional dinamical influences with respect to the CR3BP, such as the gravities of all the solar system planets, and the solar radiation pressure. Nevertheless, the restricted hypothesis is retained. Consequently, the mass of the spacecraft is assumed to have no influence on the system.

2.2.1. The Roto-Pulsating Frame

To write the equations of motion in the RPRnBP it is first necessary to define the transformations to the roto-pulsating frame (RPF), which is shown in Figure 2.2. The coordinate change from the solar system barycentric frame to the RPF is possible thanks to the following equations [7]

$$\boldsymbol{R}(t) = \boldsymbol{b}(t) + k(t)C(t)\boldsymbol{\rho}(\tau), \tag{2.13a}$$
$$\boldsymbol{V}(t) = \dot{\boldsymbol{b}} + \dot{k}C\boldsymbol{\rho} + \dot{\tau}kC\boldsymbol{\rho}', \tag{2.13b}$$
$$\tau = n(t - t_0), \tag{2.13c}$$

where primes indicate derivatives with respect to non-dimensional time, whereas dots indicate derivatives with respect to the dimensional one.

The parameters of the transformation are defined as [8]

$$\boldsymbol{b}(t) = \frac{m_1\boldsymbol{R}_1 + m_2\boldsymbol{R}_2}{m_1 + m_2}, \tag{2.14a}$$
$$k(t) = ||\boldsymbol{R}_2 - \boldsymbol{R}_1||, \tag{2.14b}$$
$$C(t) = [\boldsymbol{e}_1, \boldsymbol{e}_2, \boldsymbol{e}_3], \tag{2.14c}$$

where

$$\boldsymbol{e}_1 = \frac{\boldsymbol{R}_2 - \boldsymbol{R}_1}{k}, \qquad \boldsymbol{e}_2 = \boldsymbol{e}_3 \times \boldsymbol{e}_1, \qquad \boldsymbol{e}_3 = \frac{(\boldsymbol{V}_2 - \boldsymbol{V}_1) \times (\boldsymbol{R}_2 - \boldsymbol{R}_1)}{||(\boldsymbol{V}_2 - \boldsymbol{V}_1) \times (\boldsymbol{R}_2 - \boldsymbol{R}_1)||}. \tag{2.15}$$

These three parameters produce the three transformations needed to change reference frame. In detail:

1. $\boldsymbol{b}(t)$ produces a translation of the origin from the solar system barycenter to the center of mass of the two primaries,
2. $k(t)$ is a scaling factor, that adjusts the positions of the primaries so that they remain fixed in the RPF,
3. $C(t)$ is a rotation matrix that keeps the primaries aligned with the x-axis. As in the CR3BP, their position is fixed at $[-\mu, 0, 0]$ and $[1 - \mu, 0, 0]$, respectively.

The result is a system that rotates and pulsates in a time dependent way. The time is scaled with respect to the rotation of the primaries about the system barycenter. In fact, the scaling factor is

$$n = \sqrt{\frac{G(m_1 + m_2)}{\bar{a}^3}}, \tag{2.16}$$

where $\bar{a}$ is the mean distance between the primaries.

2.2.2. Equations of Motion

The equations of motion in the RPRnBP are written with the Lagrangian formalism. The kinetic and potential energy of the spacecraft, in the solar system barycentric frame, are respectively [7]

$$T = \frac{1}{2}\dot{\boldsymbol{R}} \cdot \dot{\boldsymbol{R}}, \tag{2.17a}$$

$$V = -\sum_{j=1}^{n} \mu_j \frac{1}{||\boldsymbol{R} - \boldsymbol{R}_j||}. \tag{2.17b}$$

The model also includes the solar radiation pressure, of which the acceleration is computed as [9]

$$\boldsymbol{a}_{SRP} = SP_0 \frac{\boldsymbol{R} - \boldsymbol{R}_S}{||\boldsymbol{R} - \boldsymbol{R}_S||^3}, \tag{2.18}$$

where SP_0 is a parameter that reads

$$SP_0 = (1 + c_r)\frac{A}{m}\frac{\Psi_0 d_0^2}{c}, \tag{2.19}$$

c_r is the reflectivity coefficient of the spacecraft, A/m its area to mass ratio, Ψ_0 the solar flux intensity at distance d_0, and c is the speed of light in vacuum.

The resulting Lagrange equations are obtained by applying the necessary condition, which leads to [7]

$$\ddot{\boldsymbol{R}} + \boldsymbol{\nabla}_R V = \boldsymbol{a}_{SRP}. \tag{2.20}$$

To compute the desired equations of motion, Equation (2.20) must be transformed into the RPF. After the transformation, the adimensional acceleration is isolated, the result being

$$\begin{aligned} \boldsymbol{\rho}'' = &\frac{1}{\dot{\tau}}\left(\frac{2\dot{k}}{k} I + 2C^T\dot{C}\right)\boldsymbol{\rho}' - \frac{1}{\dot{\tau}^2}\left[\left(\frac{\ddot{k}}{k} I + 2\frac{\dot{k}}{k} C^T\dot{C} + C^T\ddot{C}\right)\boldsymbol{\rho} + \frac{C\ddot{\boldsymbol{b}}}{k}\right] + \\ &+ \nabla\Omega + \frac{SP_0}{k^3 n^2}\frac{\boldsymbol{\rho} - \boldsymbol{\rho}_S}{||\boldsymbol{\rho} - \boldsymbol{\rho}_S||^3}, \end{aligned} \tag{2.21}$$

where Ω is the pseudo-potential of the RPRnBP, defined as

$$\Omega = \sum_{j=1}^{n} \frac{\hat{\mu}_j}{||\boldsymbol{\rho} - \boldsymbol{\rho}_j||}. \tag{2.22}$$

The equations of motion can be written by components, namely

$$x'' = b_1 + b_4 x' + b_5 y' + b_7 x + b_9 y + b_8 z + b_{13}\Omega_{/x} + a_x, \tag{2.23a}$$
$$y'' = b_2 - b_5 x' + b_4 y' + b_6 z' - b_9 x + b_{10} y + b_{11} z + b_{13}\Omega_{/y} + a_y, \tag{2.23b}$$
$$z'' = b_3 - b_6 y' + b_4 z' + b_8 x - b_{11} y + b_{12} z + b_{13}\Omega_{/z} + a_z, \tag{2.23c}$$

where $a_{x,y,z}$ are the components of the acceleration induced by the solar radiation pressure, and the b_i coefficients are [8]:

$$b_1 = -\frac{\ddot{\boldsymbol{b}} \cdot \boldsymbol{e}_1}{kn^2}, \qquad b_7 = -\frac{1}{n^2}\left(\frac{\ddot{k}}{k} - \dot{\boldsymbol{e}}_1 \cdot \dot{\boldsymbol{e}}_1\right),$$
$$b_2 = -\frac{\ddot{\boldsymbol{b}} \cdot \boldsymbol{e}_2}{kn^2}, \qquad b_8 = \frac{1}{n^2}\dot{\boldsymbol{e}}_1 \cdot \dot{\boldsymbol{e}}_3,$$
$$b_3 = -\frac{\ddot{\boldsymbol{b}} \cdot \boldsymbol{e}_3}{kn^2}, \qquad b_9 = \frac{1}{n^2}\left(2\frac{\dot{k}}{k}\boldsymbol{e}_2 \cdot \dot{\boldsymbol{e}}_1 + \boldsymbol{e}_2 \cdot \ddot{\boldsymbol{e}}_1\right),$$
$$b_4 = -\frac{2}{n}\frac{\dot{k}}{k} \qquad b_{10}, = -\frac{1}{n^2}\left(\frac{\ddot{k}}{k} - \dot{\boldsymbol{e}}_2 \cdot \dot{\boldsymbol{e}}_2\right),$$
$$b_5 = \frac{2}{n}\boldsymbol{e}_2 \cdot \dot{\boldsymbol{e}}_1, \qquad b_{11} = \frac{1}{n^2}\left(2\frac{\dot{k}}{k}\boldsymbol{e}_3\dot{\boldsymbol{e}}_2 + \boldsymbol{e}_3 \cdot \ddot{\boldsymbol{e}}_2\right),$$
$$b_6 = \frac{2}{n}\boldsymbol{e}_3 \cdot \dot{\boldsymbol{e}}_2, \qquad b_{12} = -\frac{1}{n^2}\left(\frac{\ddot{k}}{k} - \dot{\boldsymbol{e}}_3 \cdot \dot{\boldsymbol{e}}_3\right),$$
$$b_{13} = \frac{\mu_S + \mu_P}{k^3 n^2}.$$

It is interesting to note that by assuming $b_5 = 2$, $b_7 = b_{10} = b_{13} = 1$, and $b_i = 0$ for $i \neq 5, 7, 13$, one can obtain the equations of motion for the CR3BP. Thus, the CR3BP can be seen as a more particular case of the RPRnBP.

2.2.3. Linearized Model

A useful tool to propagate small variations of the initial condition is the linearized model. Let $\boldsymbol{x} = [\boldsymbol{\rho}; \boldsymbol{\eta}]$ be the state vector, containing the spacecraft position and velocity. The matrix that propagates small variations of the initial condition is the state transition matrix (STM), computed through the integration of the variational equation

$$\dot{\Phi}(t_0,t) = \frac{\partial \boldsymbol{f}}{\partial \boldsymbol{x}}\Phi(t_0,t), \qquad \Phi(t_0,t_0) = I. \tag{2.24}$$

The variational equation can be integrated together with the equations of motion, resulting in a model which features 42 scalar differential equations.

The STM is used to propagate small variations in the initial condition with the following relation:

$$\delta\boldsymbol{x}(t) = \Phi(t_0,t)\delta\boldsymbol{x}_0. \tag{2.25}$$

To integrate the variational equation it is necessary to compute the Jacobian of the right hand side, which can be expressed as

$$\frac{\partial \boldsymbol{f}}{\partial \boldsymbol{x}} = \begin{bmatrix} \dfrac{\partial \boldsymbol{f}_1}{\partial \boldsymbol{\rho}} & \dfrac{\partial \boldsymbol{f}_1}{\partial \boldsymbol{\eta}} \\ \dfrac{\partial \boldsymbol{f}_2}{\partial \boldsymbol{\rho}} & \dfrac{\partial \boldsymbol{f}_2}{\partial \boldsymbol{\eta}} \end{bmatrix}, \tag{2.26}$$

where

$$\frac{\partial \boldsymbol{f}_1}{\partial \boldsymbol{\rho}} = 0_{3\times 3}, \tag{2.27a}$$

$$\frac{\partial \boldsymbol{f}_1}{\partial \boldsymbol{\eta}} = I_{3\times 3}, \tag{2.27b}$$

$$\begin{aligned} \frac{\partial \boldsymbol{f}_2}{\partial \boldsymbol{\rho}} = &-\frac{2}{\dot{\tau}}\left(\frac{\dot{k}}{k}I + C^T\dot{C}\right) - \frac{1}{\dot{\tau}^2 k^3}\sum_{j=1}^{n}\mu_j\left(\frac{I}{||\boldsymbol{\rho}-\boldsymbol{\rho}_j||^3} - \frac{3(\boldsymbol{\rho}-\boldsymbol{\rho}_j)(\boldsymbol{\rho}-\boldsymbol{\rho}_j)^T}{||\boldsymbol{\rho}-\boldsymbol{\rho}_j||^5}\right) + \\ &+ \frac{SP_0}{\dot{\tau}^2 k^3}\left[\frac{I}{||\boldsymbol{\rho}-\boldsymbol{\rho}_j||^3} - \frac{3(\boldsymbol{\rho}-\boldsymbol{\rho}_j)(\boldsymbol{\rho}-\boldsymbol{\rho}_j)^T}{||\boldsymbol{\rho}-\boldsymbol{\rho}_j||^5}\right], \end{aligned} \tag{2.27c}$$

$$\frac{\partial \boldsymbol{f}_2}{\partial \boldsymbol{\eta}} = -\frac{2}{\dot{\tau}}\left(\frac{\dot{k}}{k}I + C^T\dot{C}\right). \tag{2.27d}$$

2.3. Periodic Orbits about Lagrangian Points

Periodic orbits about Lagrangian points can be computed thanks to the linearized model, in the CR3BP, with a semi-analytical approach. This method consists in the use of perturbation techniques to correct the initial condition, and continuation techniques to

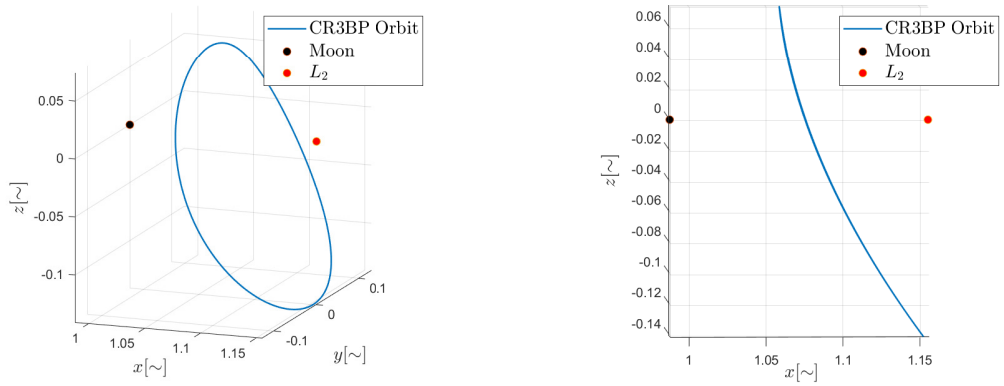

(a) Reference Orbit (b) Projection on (x, z) Plane

Figure 2.3: Reference Orbit in the CR3BP

expand the orbits [27].

Various families of orbits are created with the method. The orbit used as baseline in this work is a halo orbit about L_2, with a Jacobi constant of $C_J = 3.09$. It is represented in Figure 2.3.

2.3.1. Dynamical Substitutes of Periodic Orbits

The periodic orbits about Lagrangian points are computed in the CR3BP. However, this work is carried out in the RPRnBP. This creates the need of a reference trajectory, computed in the RPRnBP, that stays as close as possible to the seed orbit in the CR3BP. Such a trajectory can be computed with a method developed by Dei Tos and Topputo [8].

The method is divided into three steps. It starts with the generation of a seed orbit, then a correction with modified multiple-shooting, and finally interpolation/extrapolation with Fourier analysis. Specifically:

1. Generate a seed orbit, in the form of a sequence of nodes. The seed orbit comes from the CR3BP at the first iteration, and from Step 3 at further iterations.
2. For a given time span ΔT perform the modified multiple-shooting method. This is stated as a non-linear program, in which the requirement is to produce a continuous trajectory that remains as close as possible to the seed orbit. The variable of the problem is the initial condition of the trajectory, the constraints are the defects between each arc, and the objective is the minimization of the corrections with respect to the seed orbit.
3. Finally, the Fourier interpolation provides an approximation of the generated orbit.

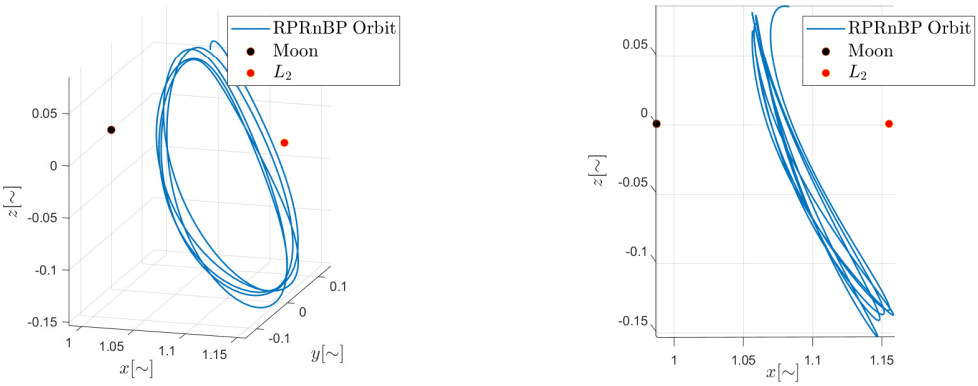

(a) Reference Orbit (b) Projection on (x, z) Plane

Figure 2.4: Reference Orbit in the RPRnBP

Since the orbit produced by the multiple-shooting will be quasi-periodic, Fourier series is the best tool for interpolation. After the interpolation, the extrapolation is necessary to provide an initial guess to repeat Step 1. When the generated trajectory stays close to the seed orbit for enough time, the process is terminated.

The trajectory used for this work is the dynamical substitute of the CR3BP orbit shown in the previous section. It is reported in Figure 2.4.

2.3.2. Local Stability

To assess the stability proprieties of the libration point orbits in the CR3BP it is sufficient to use the linearized model, which is still periodic. The most important parameters in this investigation are the eigenvalues of the Monodrimy matrix.

The Monodromy matrix is defined as the STM for one period of the orbit

$$M = \Phi(0, T). \tag{2.28}$$

The eigenvalues of M, for halo orbits, can be divided into three pairs:

- A pair of real reciprocal eigenvalues, such that $\lambda_1 \lambda_2 = 1$.
- A pair of unitary eigenvalues.
- A pair of complex conjugate eigenvalues, with norm equal to 1.

Each couple of eigenvalues has a specific geometrical meaning [19].

- The reciprocal pair (λ_1, λ_2), with $\lambda_1 > 1$, is associated with the stability characteristics of the orbit. In particular, λ_1 defines the most expanding direction of the orbit. The eigenvectors associated to the pair (λ_1, λ_2), can be used as initial guesses to compute the unstable and stable manifolds, respectively.
- The unitary pair (λ_3, λ_4) is associated with the neutral variables of the orbit. Specifically, the eigenvector of λ_3 is the tangent vector, and λ_4 is related to variations of energy/period along the family of halo orbits.
- The complex conjugate pair (λ_5, λ_6) is composed of eigenvalues of unitary norm. Geometrically, complex conjugate eigenvalues represent a rotation. This behaviour represents the existence of quasi-periodic halo orbits around the specific halo orbit.

It is important to note that the orbits in the RPRnBP are only quasi-periodic, and consequently, the monodromy matrix is not defined. It is however possible to do the same considerations, by computing the STM over a time interval close to the orbital period in the CR3BP. In this case, it can happen that the two unitary eigenalues become another complex conjugate pair, because of the loss of periodicity. For reference, the eigenvalues of the orbit used in this work are reported in Table 2.1. Note that, for numerical reasons, the unitary eigenvalues are not computed exactly, although they are equal to one up to the 11-th decimal digit.

Table 2.1: Eigenvalues of Reference Orbit

Eigenvalue	Real Part	Imaginary Part
λ_1	248.6325	0
λ_2	0.004022	0
λ_3	0.9999	0
λ_4	0.9999	0
λ_5	0.1321	0.9912
λ_6	0.1321	- 0.9912

3 | Station-Keeping Strategies

3.1. Methods Based on Dynamical Effects

The methods based on dynamical effects exploit the features of the CR3BP. As seen in Chapter 2, the monodromy matrix has one unstable eigenvalue. These methods aim at removing the unstable component in the motion of the spacecraft.

3.1.1. Floquet Mode Approach

The Floquet mode approach (FMA) exploits Floquet theory to compute and eliminate the unstable component of the motion. The computation of the unstable component requires the the integration of the variational equations to obtain the STM. However, for large time intervals, the STM can become ill-conditioned. One can take advantage of Floquet modes to express the eigenstructure of the STM, with a formalism that exploits the periodicity of the orbit, and consequently does not require long integration intervals.

The controller implemented in the Floquet modes approach aims at eliminating the influence of the unstable manifold on the motion of the spacecraft. To do so, at every maneuver point, the Δv is computed in order to cancel the unstable component of the state vector.

3.2. Methods of General Control Theory

The methods of general control theory are techniques formulated for the general control problem, applied to the station-keeping problem.

3.2.1. Target Point Approach

The target point approach (TPA) is a strategy that aims at maintaining the spacecraft in the vicinity of the reference trajectory. At each maneuver point, the controller computes the Δv in order to minimize a weighted cost function, which reads [5]

$$J = \Delta \boldsymbol{v}^T Q \Delta \boldsymbol{v} + \sum_{i=1}^{N_{TP}} \boldsymbol{d}_i^T R_i \boldsymbol{d}_i^T, \tag{3.1}$$

where Q and R_i are the weight matrices, $\boldsymbol{d}_i$ are the distances between the spacecraft and the target points, and N_{TP} is the number of target points. The cost function is defined in terms of the Δv, and the deviations in position and velocity from the reference trajectory at specific times. The points on the reference orbit at those specific epochs are called target points, and are used by the method to blend the necessity of minimizing the fuel cost, with the constraint of remaining in the vicinity of the reference trajectory.

3.2.2. Other Targeting Strategies

Other targeting strategies, different from the target point approach, have been implemented. One was considered by Pavlak and Howell [26], called short term approach (STA). In this strategy only one point is targeted, and the objective function, which is only the maneuver Δv, is minimized using the simple-shooting method. After having discretized the reference trajectory into a series of patch points, the method computes the Δv in order to connect with the following patch point, while minimizing the magnitude of the maneuver.

Another example is the orbit continuation strategy (OCS) examined by Folta et al [13]. Here the maneuvers are computed to retain the spacecraft into an orbit that is around the libration point, without following any specific reference trajectory. This is done by imposing a set of user defined constraints, in terms of the spacecraft's state, at successive crossings of the (x, z) plane.

Finally, the long term approach (LTA) was considered by Pavlak [25]. This method computes locally optimal maneuvers through direct optimization, using sequential quadratic programming. The optimization problem is stated as a multiple-shooting, in order to compute a continuous solution that meets a set of end of mission constraints.

3.2.3. Sliding Mode Control

The sliding mode control (SMC) was implemented by Lian et al. [21], in order to stabilize the spacecraft in its orbit. The framework of the method is the linearized equations of motion, discretized in time, written as [28]

$$\boldsymbol{x}(k+1) = A\boldsymbol{x}(k) + B\Delta \boldsymbol{v}(k), \tag{3.2}$$

where

$$A = \Phi(t_k, t_{k+1}), \tag{3.3a}$$
$$B = \Phi(t_k, t_{k+1})\bar{B}, \tag{3.3b}$$

with $\bar{B} = [0_{3\times3}; I_{3\times3}]$. For this strategy, the system's state is driven to the sliding surface, defined as [21]

$$\boldsymbol{\sigma} = \{\boldsymbol{x} \in R^3 | \boldsymbol{s}(\boldsymbol{x}) = \mathbf{0} \in R^3\}, \tag{3.4}$$

and remains attached to it for the rest of the motion. The sliding surface is generally written as a linear function, specifically the intersection of three hyper-planes passing through the origin. $\boldsymbol{s}$ is called switching function, and reads

$$\boldsymbol{s}(k) = C_1\boldsymbol{r}(k) + C_2\boldsymbol{v}(k), \tag{3.5}$$

where C_1 and C_2 are real square matrices, that must verify $C\boldsymbol{x}(k) = 0$ when the state reaches the sliding surface. The controller is developed in order to keep the state on the sliding surface, while minimizing a performance index, written as

$$J = \sum_{k=0}^{\infty} \boldsymbol{x}^T(k) Q \boldsymbol{x}(k). \tag{3.6}$$

The performance index is generally minimized with a discretized linear quadratic regulator control strategy.

3.2.4. Modified Chebishev-Picard Iterations

The modified Chebishev-Picard iteration method (MCPI) was applied by Xiaoli Bai et al [2]. In this method the reference trajectory is represented by means of Chebishev polynomials. The controller computes the Δv by solving a two-point boundary-value problem, using Picard iterations to refine the solution. The standard Picard iteration for a second order two-point boundary-value problem reads [1]

$$\boldsymbol{x}^{k+1} = \omega_2^2 C_x C_\alpha^B \boldsymbol{f} + C_x \Theta_{xif}, \tag{3.7}$$

where $\boldsymbol{x}^{k+1}$ is the k-th iterate of the initial state, ω_2 is a parameter, C_x and C_α^B are matrices, related to Chebishev polynomials, $\boldsymbol{f}$ is a vector of evaluations of the right hand side at different epochs, and Θ_{xif} is a matrix related to the boundary conditions. The maneuver Δv is computed through those iterations, with a problem stated in a similar way to a Lambert problem.

The main advantage of the method is the possibility of parallelization. This makes the computational time fast, enabling the distribution of tasks to different processors. Moreover, the method does not require neither gradients nor state transition matrices, making the integration time lower.

3.3. Comparison and Trade-Off

The strategies to be implemented in this work are selected thorugh a trade-off. The primary factors considered are: the fuel cost, the requirement of a reference trajectory, the frequency between maneuvers, and the dynamical model in which the strategy was implemented in previous studies. The objective is to minimize the fuel cost, consequently the choice of the Δv as a parameter is trivial. Also, the presence of a reference trajectory is considered because for mission LUMIO it is not necessary, and the relaxation of that constraint might lead to lower fuel cost. The maneuver frequency and the dynamical model are both constraints imposed by the mission. It must be noted that controlling the spacecraft is easier if the maneuvers are closer to each other, while implementing a strategy in the CR3BP leads to lower costs with respect to the RPRnBP. Table 3.1 summarizes the previously cited characteristics of the strategies.

Table 3.1: Trade-Off between Station-Keeping Strategies

Strategy	Δv [m / s / y]	Ref. Trajectory	Man. Frequency	Model
Target Point	18.3	✓	LUMIO	RPRnBP
Floquet Mode	7	✓	$1/2T$	CR3BP
Chebishev-Picard	14.7	✓	$1/7T$	CR3BP
Sliding Mode	16		6 d	RPRnBP
Short Term	N/A	✓	7 d	Ephemeris
Long Term	10	✓	7 d	Ephemeris
Orbit Continuation	35		7 d	Ephemeris

Target point approach was already implemented by Cipriano et al. [5] for LUMIO mission. Although results are already present, they can be improved by better tuning the parameters of the method.

Floquet mode approach was implemented by Cravedi [6] for orbits belonging to the same family as LUMIO, but with a higher Jacobi constant (easier to control), and with less stringent constraints on maneuver timing. Trying to implement the method with the maneuver constraints, and in the orbit of LUMIO would be of practical interest. The results given by Gomez et al. [17] show that controlling the spacecraft with the maneuver timings of LUMIO could be very difficult. However, even if controlling LUMIO with FMA turns out to be impossible, a blend between FMA and TPA could be a way to use Floquet modes to improve the fuel budget of the mission. Consequently, Floquet mode approach is selected to be investigated in this work.

The main advantage offered by modified Chebishev Picard iteration method is the computational efficiency, because of the ease of parallelization and the absence of variational equations. Since the computation of LUMIO's maneuvers is done by the ground segment and not onboard, the advantage in efficiency is not considered crucial for the mission. Consequently the strategy is discarded.

Sliding mode control was tested on an orbit with $C_J = 3.14$. A higher Jacobi constant means that the periodic nature of the CR3BP orbit is more preserved, leading to easier controllability with a linearized model. Although the strategy has a promising fuel cost, the paper suggests high sensitivity to tracking errors. The fact that the errors used in the paper are lower with respect to the ones of LUMIO, and the orbit is more favourable, one can assume that the results applied to LUMIO would be worse. For these facts, the strategy is not selected.

The paper by Pavlak and Howell [26] does not report the resulting fuel cost for the short term approach. However, it presents the strategy as viable for halo orbits, also in the ephemeris model, which is more complex than the CR3BP. It is considered of interest to find numerical results for the method applied to LUMIO mission.

The long term approach has one of the best fuel costs of the list. One issue is that it was tested on the ARTEMIS mission, which was on a Lissajous trajectory, instead of a halo. The other important feature of the method is the ability to target end of life constraints, which are not of practical interest for LUMIO mission. The method was thus discarded.

As long term approach, orbit continuation strategy was applied to ARTEMIS mission. In addition to that, the strategy requires user defined constraints to extend the orbit. Writing such constraints requires extensive tuning campaigns of the parameters. For those reasons the method was not taken into consideration.

In conclusion, target point approach, Floquet modes approach and short term approach

were selected for this work. TPA may be improved by better tuning the parameters, FMA needs to be tested in the RPRnBP, and may be blended with TPA, and STA needs to be implemented to see its performances.

4 | Target Point Approach

4.1. Station-Keeping Problem

After the spacecraft is injected onto the nominal orbit, it is necessary to implement maneuvers that keep the satellite close to its reference trajectory. In fact, without any correction, a vehicle on a libration point orbit would diverge from the desired path, due to the unstable dynamics and the perturbations from the other bodies in the solar system.

Although it is impossible to keep the spacecraft exactly on the reference orbit, one can aim at enclosing the motion inside a torus, centred about the nominal trajectory. The objective of the station-keeping problem is to bind the motion of the spacecraft into the torus, while respecting constraints and optimizing performance indexes.

In the case of LUMIO mission, which is the case study analyzed in this work, the main performance index considered is the fuel cost. The constraints, on the other hand, are related to the time between maneuvers and the maximum deviation, which have been fixed in the mission analysis.

4.2. Operation Errors

Three potential sources of error were considered for the analysis:

1. Orbit injection error. The spacecraft arrives on the reference trajectory thanks to an orbit insertion maneuver. However, the injection cannot be perfect, and this fact has to be modeled. To do this, each component of the initial state is perturbed independently at the beginning of the simulation.

2. Orbit determination error. During the mission the state of the spacecraft is not known exactly. In fact, it is determined by the camera of the satellite, that inherently has an error in its measurements. Hence, each tracking campaign is simulated as a perturbation of the real state.

3. Maneuver execution error. Each time a station-keeping maneuver is computed, it

has to be executed by the engine. As the other processes explained before, the engine has a degree of inaccuracy, both in the magnitude of the burn and in the pointing. Consequently, an element of randomness is added to the Δv of the maneuver.

The first two sources of error are modeled as a random number, that respects a Gaussian distribution. The distribution is constructed with zero mean, and a variance dictated by the precision of the maneuver or the tracking device, respectively. In contrast, the maneuver execution error represents a percentage of the Δv computed.

4.3. Representation of the Nominal Orbit

This station keeping strategy does not require to propagate the actual state of the spacecraft. In fact, propagating only the deviations from the nominal orbit is enough. This requires the STM to be available at any given time along the reference trajectory.

The output files from the orbit generation contain the state and the STM only at specific epochs. A solution would be to integrate the variational equation during the station-keeping simulation, but it would massively increase the computational cost. For this reason, the values of the STM generated together with the orbit are used to create an interpolation. Cubic splines are exploited to approximate both the reference trajectory and the STM. This method requires negligible computational time, while still retaining a high degree of accuracy [19].

4.4. Station-Keeping Strategy

Target point approach computes the maneuver Δv by minimizing a weighted cost function J. The function is constructed to combine the magnitude of the impulse with the deviation from the reference trajectory. The latter is computed as the distance between the spacecraft and some target points at a future epoch, and reads

$$J = \Delta \boldsymbol{v}^T Q \Delta \boldsymbol{v} + \sum_{i=1}^{N_{TP}} \boldsymbol{d}_i^T R_i \boldsymbol{d}_i^T, \tag{4.1}$$

where $\boldsymbol{d}_i$ is the predicted deviation at the i-th target point, N_{TP} is the number of target points considered, and Q and R_i are the weighting matrices. The deviation from the reference trajectory is predicted through the STM, as

$$\boldsymbol{d}_i = \Phi_{rr}(t_c, t_i)\delta \boldsymbol{r}_c + \Phi_{rv}(t_c, t_i)\delta \boldsymbol{v}_c + \Phi_{rv}(t_v, t_i)\Delta \boldsymbol{v}, \tag{4.2}$$

where the subscripts r and v are referred to 3-by-3 components of Φ, that map position and velocity deviations to a successive position deviation, respectively. In addition, t_c is the cutoff time, t_v is the maneuver execution epoch, and t_i is the epoch of the i-th target point.

The expression of the maneuver Δv derives from the minimization of the cost function, as a solution of an LQR problem. It reads [5]

$$\Delta \boldsymbol{v} = A \sum_{i=1}^{N_{TP}} \alpha_i \delta \boldsymbol{r}_c + \beta_i \delta \boldsymbol{v}_c, \tag{4.3}$$

where A, α_i, and β_i are defined as

$$A = -\left[\left(Q^T + Q \right) + \sum_{i=1}^{N_{TP}} \Phi_{rv}^T(t_v, t_i) \left(R_i^T + R_i \right) \Phi_{rv}(t_v, t_i) \right]^{-1}, \tag{4.4a}$$

$$\alpha_i = \Phi_{rv}^T(t_v, t_i) \left(R_i^T + R_i \right) \Phi_{rr}(t_c, t_i), \tag{4.4b}$$

$$\beta_i = \Phi_{rv}^T(t_v, t_i) \left(R_i^T + R_i \right) \Phi_{rv}(t_c, t_i). \tag{4.4c}$$

4.5. Station-Keeping Algorithm

The station-keeping algorithm simulates the real mission scenario. It starts when the spacecraft is injected into the reference orbit, and goes on until either the final time or the maximum deviation is reached. If the simulation ends because of the maximum deviation constraints, the station-keeping is failed.

The algorithm can be summarized as:

1. Start the simulation with the initial deviation being equal to the orbit injection error.
2. Propagate the deviation, through the STM, until the cutoff time. Here add the orbit determination error to the deviation. Store the true and the perturbed state as two different vectors.
3. Propagate both the true and the perturbed state until maneuver time.
4. Compute the maneuver with the perturbed state, but apply the maneuver to the true state.
5. Add maneuver execution error to the Δv.

Algorithm 4.1 Station-Keeping Algorithm with Target Point Approach

function DV($t_0, t_f, \Phi, \Delta t_c, \Delta t_v, \Delta t_i, \sigma^2_{OI}, \sigma^2_{OD}, \sigma^2_{EX}, Q, R$)
$t \leftarrow t_0$
Generate Orbit Insertion Error: $\boldsymbol{\varepsilon}_{OI} \sim \mathcal{N}(0, \sigma^2_{OI})$
Orbit Insertion: $\delta\boldsymbol{x}_{true} \leftarrow \boldsymbol{\varepsilon}_{OI}$
while $t \leq t_f$ & $\delta\boldsymbol{x}_{true} \leq 10000$ km **do**
  $t_v \leftarrow t + \Delta t_v$
  $t_c \leftarrow t + \Delta t_c$
  $t_i \leftarrow t + \Delta t_i$
  if $t_i \geq t_{end}$ **then**
    $t_i \leftarrow t_{end}$
  end if
  Propagate to Cutoff Time: $\delta\boldsymbol{x}_{true} \leftarrow \Phi(t_c, t)\delta\boldsymbol{x}_{true}$
  Generate Orbit Determination Error: $\boldsymbol{\varepsilon}_{OD} \sim \mathcal{N}(0, \sigma^2_{OD})$
  Orbit Determination: $\delta\boldsymbol{x}_{OD} \leftarrow \delta\boldsymbol{x}_{true} + \boldsymbol{\varepsilon}_{OD}$
  Plan Maneuver: $\Delta\boldsymbol{v} = A\sum_{i=1}^{N_{TP}} \alpha_i\delta\boldsymbol{r}_{OD} + \beta_i\delta\boldsymbol{v}_{OD}$
  Propagate to Maneuver Execution: $\delta\boldsymbol{x}_{true} = \Phi(t_c, t_v)\delta\boldsymbol{x}_{true}$
  Generate Maneuver Execution Error: $\boldsymbol{\varepsilon}_{EX} \sim \mathcal{N}(0, \sigma^2_{EX})$
  Perturb Maneuver Δv: $\Delta\boldsymbol{v} \leftarrow \Delta\boldsymbol{v} \circ \boldsymbol{\varepsilon}_{EX}$
  Execute Maneuver: $\delta\boldsymbol{x}_{true} \leftarrow \delta\boldsymbol{x}_{true} + [0_{3\times1}; \Delta\boldsymbol{v}]$
  $t \leftarrow t_v$
end while
end function

6. Repeat steps 2 to 5 until the final time is reached, or until the maximum deviation is surpassed.

The algorithm can also be written in the form of a pseudo-algorithm, which is reported as Algorithm 4.1.

4.6. Monte-Carlo Analysis

The station-keeping algorithm presented in the previous section would not generate significant results with a single simulation. This is because the operation errors are generated as a random number, which respects a normal distribution. For this reason, it is not possible to obtain an analytical result for the station-keeping problem. Although not analytical, if the simulation is ran multiple times, the results can become statistically significant. This is why a Monte-Carlo simulation is necessary to evaluate the effectiveness of a strategy.

To produce a Monte-Carlo analysis, the simulation is ran multiple times, to generate different samples, each one different from the other because of the randomness of the operation errors. The results of the analysis are to be intended as mean Δv to keep the

spacecraft bounded to the reference orbit. Together with the mean, the range spanned by the Δv is also an important performance parameter, because it represents the robustness and the reliability of the strategy. The results of this work are obtained with 10000 samples, as in the main literature sources [17].

4.7. Objectives of the Analysis

The target point approach was already tested for LUMIO by Cipriano et al. [5], and improved by Dei Tos and Baresi [32], as baseline station-keeping strategy, and was proved to be successful. Provided the effectiveness of the strategy, there is still room for improvement. This analysis has two main objectives regarding target point approach.

First, in the work by Cipriano et al. [5], the orbit determination errors are treated as instantaneous displacements of the spacecraft. After the addition of the orbit determination error the true state is lost, and the perturbed state becomes the real one. This hypothesis is dropped in this work, as the state affected by the orbit determination error is used to compute the maneuver. The Δv computed is then applied to the real state.

The second objective is to improve the tuning of the parameters. Considering that maneuver timing is a constraint imposed by the mission analysis, particular focus is given to the epochs of the two target points. The weight matrices are finally considered, to test their impact on the performances of the strategy.

5 | Floquet Modes Approach

Floquet modes approach aims at keeping the spacecraft onto the reference orbit by removing the component of the state vector associated with the unstable manifold. To do so, it is necessary to have information about the eigenvectors of the STM at every epoch. Even though the orbits in the CR3BP are perfectly periodic, the STM does not retain that feature. In fact, considering the rules for propagation of the STM, its element exponentially increase with time

$$\Phi(t_0, nt) = \Phi^n(t_0, t).$$

Floquet theory comes in handy, because it introduces a formalism in which the eigenvectors of the STM are written in a periodic manner. Although orbits in the RPRnBP are not periodic, Floquet theory can still be used provided some assumptions are taken, which are better explained in the following sections.

5.1. Computation of Floquet Modes

Floquet theory is formulated in the CR3BP , where the orbits are perfectly periodic. In that model, the STM is a fundamental matrix, and can thus be decomposed into the product of a T periodic matrix E and an exponential matrix [35]

$$\Phi(t_0, t) = E(t_0, t)e^{Jt}. \tag{5.1}$$

Post-multiplying both sides by a constant real square matrix S, one can obtain

$$\tilde{\Phi}(t_0, t) = \tilde{E}(t_0, t)e^{\tilde{J}t}, \tag{5.2}$$

where $\tilde{\Phi}(t_0, t)$ and $\tilde{E}(t_0, t)$ are simply

$$\tilde{\Phi}(t_0, t) = \Phi(t_0, t)S, \qquad \tilde{E}(t_0, t) = E(t_0, t)S. \tag{5.3}$$

After a quick demonstration [19], matrix $\tilde{J}$ can be computed as

$$\tilde{J} = S^{-1}JS.$$

It can be shown that the monodromy matrix can be diagonalized with matrices S and $\tilde{J}$, the results being

$$M = Se^{-\tilde{J}T}S^{-1}. \tag{5.4}$$

Because of this, matrix S has to contain the eigenvectors of M, and $\tilde{J}$ has to contain the Poincarè exponents of M. The The final expression of Floquet modes is

$$\tilde{E}(t_0, t) = \Phi(t_0, t)Se^{-\tilde{J}t}, \qquad t \in [0, T]. \tag{5.5}$$

Matrix S is simply computed as the eigenvectors of the monodromy matrix. To cope with the fact that M has a complex conjugate pair, it can be rewritten as

$$S = [\boldsymbol{s}_1, \boldsymbol{s}_2, \boldsymbol{s}_3, \boldsymbol{s}_4, \mathrm{Re}\{\boldsymbol{s}_5\}, \mathrm{Im}\{\boldsymbol{s}_5\}]. \tag{5.6}$$

In addition, considering that the model of this work is the RPRnBP, it can happen that the two unitary eigenvalues become complex conjugate, because of the loss of periodicity. In that case, matrix S is

$$S = [\boldsymbol{s}_1, \boldsymbol{s}_2, \mathrm{Re}\{\boldsymbol{s}_3\}, \mathrm{Im}\{\boldsymbol{s}_3\}, \mathrm{Re}\{\boldsymbol{s}_5\}, \mathrm{Im}\{\boldsymbol{s}_5\}]. \tag{5.7}$$

Matrix $\tilde{J}$, on the other hand, requires the computation of the Poincarè exponents. These are function of the eigenvalues of the monodromy matrix, in general defined as

$$\omega_i = \frac{1}{T} \ln \lambda_i. \tag{5.8}$$

In the case of a complex eigenvalue, which can be written as $\lambda_i = a_i + jb_i$, the Poincarè exponent is also complex, namely

$$\omega_i = r_i + j\theta_i, \tag{5.9}$$

where

$$r_i = \frac{1}{T}\ln\left(\sqrt{a^2+b^2}\right),$$
$$\theta_i = \frac{1}{P}\tan^{-1}\left(\frac{b}{a}\right).$$

Matrix $\tilde{J}$ is finally assembled in diagonal blocks

$$\tilde{J} = \left[\begin{array}{cc|cc|cc} r_1 & 0 & & & & \\ 0 & r_2 & & & & \\ \hline & & r_3 & \theta_3 & & \\ & & -\theta_3 & r_3 & & \\ \hline & & & & r_5 & \theta_5 \\ & & & & -\theta_5 & r_5 \end{array}\right]. \tag{5.11}$$

5.2. Station-Keeping Using Floquet Modes

After having computed the Floquet modes for the orbit, it is necessary to develop a controller that exploits them to keep the spacecraft onto the reference trajectory. This is done by computing maneuvers that cancel the unstable component of the state vector.

For this analysis two types of controllers were considered: the first one investigated by Gomez et al. [17], and the second implemented by Keeter [19]. For both the controllers the 3-axis version was selected, in order to counteract the perturbations given by the solar system planets, which are present in the RPRnBP, and are strong especially on the z axis.

5.2.1. First Controller

The first controller is the one analyzed by Gomez [17]. At any epoch along the orbit, the state error vector can be expressed as a linear combination of the Floquet modes

$$\delta\boldsymbol{x}(t) = \sum_{i=1}^{6} \alpha_i \tilde{\boldsymbol{e}}_i. \tag{5.12}$$

Assuming that the first vector of the basis is the one associated with the unstable manifold,

the objective of the controller is to annihilate the magnitude of α_1. To do so, it is first necessary to define a matrix that substitutes the unstable Floquet mode with the error vector, as

$$\tilde{E}_{unst} = [\delta\boldsymbol{x}, \tilde{\boldsymbol{e}}_2, \dots, \tilde{\boldsymbol{e}}_6]. \tag{5.13}$$

Hence, the unstable component reads

$$\alpha_1 = \frac{\det(\tilde{E}_{unst})}{\det(\tilde{E})}. \tag{5.14}$$

The unstable component can also be written as the scalar product between the error vector and the projection factors π_i, the results being

$$\alpha_1 = \pi_1\delta x + \cdots + \pi_6\delta\dot{z} = \boldsymbol{\pi}\cdot\delta\boldsymbol{x}. \tag{5.15}$$

The projection factors are necessary for the controller Δv, and can be computed as

$$\pi_i = \frac{C_{i,1}(\tilde{E}_{unst})}{\det(E)}, \tag{5.16}$$

where $C_{i,1}$ is the cofactor computed by eliminating the i-th row and the first column from $\tilde{E}_{unst}$ matrix.

The maneuver Δv is computed by imposing the annihilation of the unstable component, which requires $(\delta\boldsymbol{x} + \delta\boldsymbol{v})\cdot\boldsymbol{\pi} = 0$. This leads to the controller equation, which is

$$\Delta_x\pi_4 + \Delta_y\pi_5 + \Delta_z\pi_6 + \alpha_1 = 0. \tag{5.17}$$

The controller equation is undetermined, although one can still find an optimal solution, by minimizing the norm of $\Delta\boldsymbol{v}$. Such solution reads [17]

$$\Delta_x = -\frac{\alpha_1\pi_4}{\pi_4^2+\pi_5^2+\pi_6^2}, \qquad \Delta_y = -\frac{\alpha_1\pi_5}{\pi_4^2+\pi_5^2+\pi_6^2}, \qquad \Delta_z = -\frac{\alpha_1\pi_6}{\pi_4^2+\pi_5^2+\pi_6^2}. \tag{5.18}$$

5.2.2. Second Controller

The second and last controller analyzed is the one considered by Keeter [19]. To exploit this controller, it is necessary to project the error vector $\delta\boldsymbol{x}$ onto the Floquet basis. This is done by multiplying the vector by projection matrices

$$\delta\boldsymbol{x}_i = \Pi_i \delta\boldsymbol{x}, \tag{5.19}$$

where $\delta\boldsymbol{x}_i$ is the component associated with the i-th vector in the Floquet basis, and the projection matrices read

$$\Pi_i = \frac{\tilde{\boldsymbol{e}}_i \tilde{\boldsymbol{e}}_i^T}{\tilde{\boldsymbol{e}}_i^T \tilde{\boldsymbol{e}}_i}. \tag{5.20}$$

Therefore, $\delta\boldsymbol{x}_1$ is the unstable component of the error vector.

The controller is designed in order to implement a maneuver that eliminates the unstable component. The maneuver Δv can be written as

$$\Delta\boldsymbol{v} = [0_{3\times1}, \delta\boldsymbol{v}] = [0, 0, 0, \Delta_x, \Delta_y, \Delta_z]^T. \tag{5.21}$$

Additionally, the equation that expresses the controller objective is

$$\delta\boldsymbol{x}_1 + \Delta\boldsymbol{v} = \alpha_2\delta\boldsymbol{x}_2 + \alpha_3\delta\boldsymbol{x}_3 + \alpha_4\delta\boldsymbol{x}_4 + \alpha_5\delta\boldsymbol{x}_5 + \alpha_6\delta\boldsymbol{x}_6, \tag{5.22}$$

where α_i are unknown coefficients, and the equation means that the error vector has in fact no component in the unstable direction after the maneuver has been applied. It can be helpful to rewrite Equation (5.22) in state-space components:

$$\begin{Bmatrix} \delta\boldsymbol{x}_{1_x} \\ \delta\boldsymbol{x}_{1_y} \\ \delta\boldsymbol{x}_{1_z} \\ \delta\boldsymbol{x}_{1_{\dot{x}}} \\ \delta\boldsymbol{x}_{1_{\dot{y}}} \\ \delta\boldsymbol{x}_{1_{\dot{z}}} \end{Bmatrix} + \begin{Bmatrix} 0 \\ 0 \\ 0 \\ \Delta_x \\ \Delta_y \\ \Delta_z \end{Bmatrix} = \begin{bmatrix} \delta\boldsymbol{x}_{2_x} & \dots & \delta\boldsymbol{x}_{6_x} \\ \delta\boldsymbol{x}_{2_y} & \ddots & \\ \delta\boldsymbol{x}_{2_z} & \vdots & \vdots \\ \delta\boldsymbol{x}_{2_{\dot{x}}} & & \\ \delta\boldsymbol{x}_{2_{\dot{y}}} & \ddots & \\ \delta\boldsymbol{x}_{2_{\dot{z}}} & \dots & \delta\boldsymbol{x}_{6_{\dot{z}}} \end{bmatrix} \begin{Bmatrix} \alpha_2 \\ \alpha_3 \\ \alpha_4 \\ \alpha_5 \\ \alpha_6 \end{Bmatrix}. \tag{5.23}$$

The solution of the equation, however, is not trivial, because the unknowns are the α_i

coefficients and the components of the maneuver Δv, which are more numerous than the equations. An exact solution exists for the one-axis controller, which may be enough to control the spacecraft in the CR3BP. Since this analysis is carried out in the RPRnBP, it is necessary to develop the expression of the three-axis controller, which requires an optimization.

First, Equation (5.22) has to be rewritten to isolate the unstable component. This reads

$$\delta \boldsymbol{x}_1 = \tilde{E}^* \boldsymbol{\alpha}^*, \tag{5.24}$$

which in state space components is written as

$$\begin{Bmatrix} \delta \boldsymbol{x}_{1_x} \\ \delta \boldsymbol{x}_{1_y} \\ \delta \boldsymbol{x}_{1_z} \\ \delta \boldsymbol{x}_{1_{\dot{x}}} \\ \delta \boldsymbol{x}_{1_{\dot{y}}} \\ \delta \boldsymbol{x}_{1_{\dot{z}}} \end{Bmatrix} = \left[\begin{array}{ccc|ccc} \delta \boldsymbol{x}_{2_x} & \dots & \delta \boldsymbol{x}_{6_x} & 0 & 0 & 0 \\ \delta \boldsymbol{x}_{2_y} & \ddots & & 0 & 0 & 0 \\ \delta \boldsymbol{x}_{2_z} & \vdots & \vdots & 0 & 0 & 0 \\ \hline \delta \boldsymbol{x}_{2_{\dot{x}}} & & & -1 & 0 & 0 \\ \delta \boldsymbol{x}_{2_{\dot{y}}} & \ddots & & 0 & -1 & 0 \\ \delta \boldsymbol{x}_{2_{\dot{z}}} & \dots & \delta \boldsymbol{x}_{6_{\dot{z}}} & 0 & 0 & -1 \end{array}\right] \begin{Bmatrix} \alpha_2 \\ \alpha_3 \\ \alpha_4 \\ \alpha_5 \\ \alpha_6 \\ \Delta_x \\ \Delta_y \\ \Delta_z \end{Bmatrix}. \tag{5.25}$$

The system cannot be inverted because the matrix $\tilde{E}^*$ is not square. It is however possible to write a minimization problem, which is

$$\min_{\boldsymbol{\alpha}^*} ||\boldsymbol{\alpha}^*||_Q^2, \tag{5.26}$$

subject to the constraint:

$$g(\boldsymbol{\alpha}^*) = \tilde{E}^* \boldsymbol{\alpha}^* - \delta \boldsymbol{x}_1 = 0. \tag{5.27}$$

In words, it is required that the Q-norm of the vector $\boldsymbol{\alpha}^*$ is minimized, such that the unstable component of the state vector is removed. The matrix Q is a weighting matrix that provides more flexibility to the strategy. The minimization problem can be solved analytically using Lagrange multipliers, leading to the following necessary conditions:

$$\begin{cases} \boldsymbol{\alpha}^* & = -\frac{1}{2} Q^{-1} \tilde{E}^{*T} \boldsymbol{p}, \\ \delta \boldsymbol{x}_1 & = -\frac{1}{2} \tilde{E}^* Q^{-1} \tilde{E}^{*T} \boldsymbol{p}, \end{cases} \tag{5.28}$$

where $\boldsymbol{p}$ is the vector of Lagrange multipliers. Solving the second equation for $\boldsymbol{p}$ and substituting into the first, one obtains

$$\boldsymbol{\alpha}^* = Q^{-1} \tilde{E}^{*T} \left(\tilde{E}^* Q^{-1} \tilde{E}^{*T} \right)^{-1} \delta \boldsymbol{x}_1, \tag{5.29}$$

which is the solution of the problem. The last three components of $\boldsymbol{\alpha}^*$ are the Δv computed by the controller.

5.3. Station-Keeping Algorithm

The station-keeping algorithm used for Floquet modes approach mimics the one used for target point approach, although there are some differences. The first trivial one is that the maneuvers are computed with one of the two controllers presented before, whereas the main difference is the initialization process.

The STM is necessary to compute the Floquet modes, together with matrices S and $\tilde{J}$. The state transition matrix is stored as a spline and is available at any epoch, as in target point approach. Matrices S and $\tilde{J}$, on the other hand, are computed before the station-keeping simulation, and don't require any kind of interpolation, because they are the same for the whole orbit. They do require another kind of attention though. In fact, in the RPRnBP the orbits are not periodic. To cope with this fact, the matrices are computed for every quasi-orbit. The definition of a quasi-orbit is arbitrary, but for the sake of this work, the boundaries of the quasi-orbits were set at crossings of the (x, z) plane.

5.4. Objectives of the Analysis

The objective of the analysis is to test Floquet modes approach as a backup to target point approach. The results closest to the framework of this work are the ones obtained by Gomez et al [17]. In their analysis, the performances of target point approach are better than the ones of Floquet modes approach. In addition, they also used a reference trajectory with a higher Jacobi constant, which is less favourable for TPA but more favourable for FMA, as its periodic characteristics are more maintained.

Given those premises, it is still interesting to investigate the degree of controllability that Floquet modes approach can provide to a mission like LUMIO. Even though FMA is probably not going to be able to control the spacecraft for the entire mission, the strategy can be experimented as blended with TPA. It is important to remember that Floquet modes approach is a strategy built to counteract the influence of the unstable manifold. However, in the RPRnBP, the influence of the other solar system planets is also present, although not clearly modeled into the eigenvectors of the monodromy matrix. An experiment with the first few maneuvers computed with FMA, and the other with TPA will be made to see if Floquet modes approach gives cost effective maneuvers until the instability given by the solar system planets builds up.

6 | Short Term Approach

The last strategy implemented in this work is the short term approach, described by Pavlak and Howell [26]. The goal of the strategy is to design fuel optimal maneuvers, that keep the spacecraft near the reference trajectory for a short time span, in the order of one or two periods. This is done exploiting the simple-shooting technique, and by targeting a single target point. The idea of the strategy is graphically presented in Figure 6.1.

6.1. Simple-Shooting

The simple-shooting method is used to minimize the maneuver Δv, while meeting certain constraints at the end of the trajectory. The goals are expressed in terms of the position of a target point. The problem is stated as a non linear program, in which the vector of optimization variables comprises the maneuver Δv and the final epoch. It reads

$$\boldsymbol{y} = [\Delta \boldsymbol{v}; \tau_f]. \tag{6.1}$$

As already mentioned, the aim is to design fuel-optimal maneuvers. This is done by stating an objective function which is simply the squared norm of the maneuver Δv,

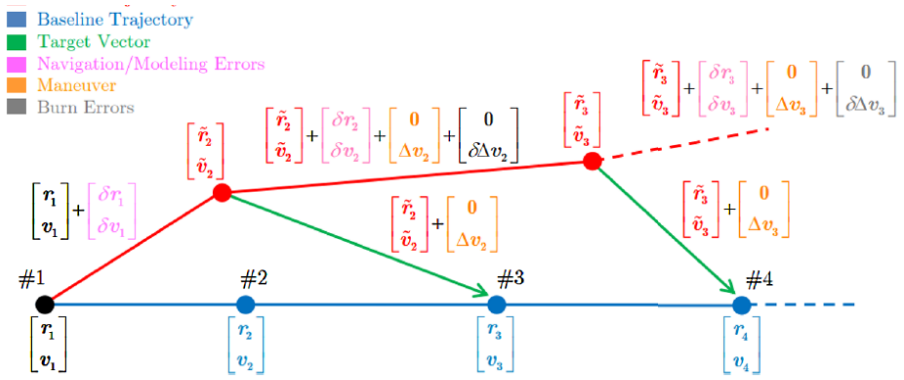

Figure 6.1: Graphical Representation of the Short Term Approach Strategy [28]

namely

$$J = ||\Delta \boldsymbol{v}||^2. \tag{6.2}$$

The norm of the maneuver Δv is squared to have a convex function, which is useful when solving the problem with gradient-based methods. Hence, the optimization is stated as a non linear program:

$$\min_{\boldsymbol{y}} J(\boldsymbol{y}), \qquad \text{s.t.} \qquad \boldsymbol{g}(\boldsymbol{y}) = 0, \tag{6.3}$$

where $\boldsymbol{g}(\boldsymbol{y})$ represents the vector of equality constraints. Such constraints are needed in order to meet the target point at the final time, and are defined as

$$\boldsymbol{g}(\boldsymbol{y}) = \boldsymbol{\varphi}_r(\boldsymbol{x}^+, \tau_{man}, \tau_f) - \boldsymbol{r}_{TP}, \tag{6.4}$$

where $\boldsymbol{x}^+ = \boldsymbol{x}^- + [0_{3\times1}; \Delta \boldsymbol{v}]$ is the state vector to which the maneuver Δv is added, and $\boldsymbol{x}^-$ is the state before the maneuver. The goal is to make a maneuver that meets the target point at a certain future epoch, in fact τ_{man} is the maneuver epoch, and τ_f is the final time of the trajectory, which is a variable of the problem.

To improve the convergence of the optimization, it is important to provide the solver with the Jacobians of the functions [9]. The first is trivially computed as

$$\frac{\partial J}{\partial \boldsymbol{y}} = \begin{Bmatrix} 2\Delta_x \\ 2\Delta_y \\ 2\Delta_z \\ 0 \end{Bmatrix}. \tag{6.5}$$

The second requires to compute the derivatives of the flow, with respect to the initial state and the final time, namely

$$\frac{\partial \boldsymbol{g}}{\partial \boldsymbol{y}} = \begin{bmatrix} \dfrac{\partial \boldsymbol{\varphi}_r}{\partial \Delta \boldsymbol{v}} & \dfrac{\partial \boldsymbol{\varphi}_r}{\partial \tau_f} \end{bmatrix}, \tag{6.6}$$

where

$$\frac{\partial \boldsymbol{\varphi}_r}{\partial \Delta \boldsymbol{v}} = \Phi_{rv}(t, t_f), \tag{6.7a}$$

$$\frac{\partial \boldsymbol{\varphi}_r}{\partial \tau_f} = \boldsymbol{f}_r(\boldsymbol{\varphi}(\boldsymbol{x}^+, t, t_f), t_f), \tag{6.7b}$$

where the subscripts r and v indicate the parts of the vectors or matrices associated with the position and velocity, respectively. The optimization problem can be solved with the MATLAB solver fmincon. As suggested in the work of Folta et al. [14], the chosen optimization algorithm is sequential quadratic programming.

6.2. Station-Keeping Strategy

The strategy implemented in the short term approach is similar to the one of target point approach. However, the minimization of the weighted cost function is substituted by the direct optimization of the maneuver Δv. The part of the cost function related to the position deviation is replaced with a non-linear equality constraint. The other main difference is that, for this approach, the error vector is not a sufficient information, and the full propagation of the state of the spacecraft is required.

Although similar to target point approach, it is useful to summarize the algorithm to highlight the differences. The main steps of the algorithm are explained hereafter, and Algorithm (6.1) is the pseudo-algorithm associated with short term approach.

1. Initialize the simulation by adding the orbit insertion errors to the initial state.
2. Propagate the state, by integrating the equations of motion, until cut-off time.
3. Perform tracking by adding the orbit determination error to the propagated state.
4. Propagate true and perturbed state to maneuver execution epoch.
5. Compute maneuver using the perturbed state, with the simple-shooting method.
6. Add maneuver execution error and execute maneuver, adding the Δv to the real state.
7. Repeat steps 2 to 6 until final time is reached.

6.3. Objective of the Analysis

The main objective of the analysis is to test this station-keeping strategy on the case study of LUMIO. This is because there are no result available for the method on halo

Algorithm 6.1 Station-Keeping Algorithm with Short Term Approach

function DV($t_0, t_f, \Phi, \Delta t_c, \Delta t_v, \Delta t_i, \sigma^2_{OI}, \sigma^2_{OD}, \sigma^2_{EX}$)
$t \leftarrow t_0$
Generate Orbit Insertion Error: $\boldsymbol{\varepsilon}_{OI} \sim \mathcal{N}(0, \sigma^2_{OI})$
Orbit Insertion: $\boldsymbol{x}_{true} \leftarrow \boldsymbol{x}_0 + \boldsymbol{\varepsilon}_{OI}$
while $t \leq t_f$ & $\delta \boldsymbol{x}_{true} \leq 10000$ km **do**
  $t_v \leftarrow t + \Delta t_v$
  $t_c \leftarrow t + \Delta t_c$
  $t_i \leftarrow t + \Delta t_i$
  if $t_i \geq t_{end}$ **then**
    $t_i \leftarrow t_{end}$
  end if
  Propagate to Cutoff Time: $\boldsymbol{x}_{true} \leftarrow \boldsymbol{\varphi}(\boldsymbol{x}_{true}, t, t_c)$
  Generate Orbit Determination Error: $\boldsymbol{\varepsilon}_{OD} \sim \mathcal{N}(0, \sigma^2_{OD})$
  Orbit Determination: $\boldsymbol{x}_{OD} \leftarrow \boldsymbol{x}_{true} + \boldsymbol{\varepsilon}_{OD}$
  Propagate to Maneuver Execution:
  $\boldsymbol{x}_{true} = \boldsymbol{\varphi}(\boldsymbol{x}_{true}, t_c, t_v)$
  $\boldsymbol{x}_{man} = \boldsymbol{\varphi}(\boldsymbol{x}_{OD}, t_c, t_v)$
  Plan Maneuver: $\Delta \boldsymbol{v} = \text{simpleShooting}(\boldsymbol{x}_{man}, \boldsymbol{x}_{TP})$
  Generate Maneuver Execution Error: $\boldsymbol{\varepsilon}_{EX} \sim \mathcal{N}(0, \sigma^2_{EX})$
  Perturb Maneuver Δv: $\Delta \boldsymbol{v} \leftarrow \Delta \boldsymbol{v} \circ \boldsymbol{\varepsilon}_{EX}$
  Execute Maneuver: $\boldsymbol{x}_{true} \leftarrow \boldsymbol{x}_{true} + [0_{3\times1}; \Delta \boldsymbol{v}]$
  $t \leftarrow t_v$
end while
end function

orbits. The method can be considered as a variation of the target point approach, since it features a similar kind of algorithm. It is interesting to compare an optimization based on a weighted cost function with one based directly on the minimization of Δv, where the target point is imposed as a constraint.

In contrast to Floquet modes approach, which is not suitable as a baseline strategy, and has to be blended with TPA, short term approach could turn out to be cheaper than TPA when considering fuel cost. It depends on the effectiveness of the direct optimization of the maneuver Δv. The results of the simulations will tell if STA is suitable as a baseline strategy.

7 | Results

7.1. LUMIO Mission

LUMIO is a mission planned for the lunar environment, which aims at studying the flux of meteoroid impacting the lunar surface. It will be carried out by a 12U form-factor CubeSat, equipped with LUMIO-cam, its main instrument.

Meteoroids collide with the lunar surface with high kinetic energy, which is partitioned into four components: production of seismic waves, formation of a crater, ejection of particles and emission of radiation. LUMIO-cam is designed to detect impact flashes, while observing a large portion of the lunar surface.

Studying the flux of meteoroid impacts is of scientific interest, because they can improve our knowledge about near-Earth objects, and the formation of the solar system. Moreover, characterization of impacts is also vital for the design of space based assets, particularly their shields. Finally, the impacts with larger near Earth objects, although rare, pose a significant threat to life on Earth, and studying their population can be vital for mitigation actions.

Doing this research with a satellite allows to exploit numerous advantages, such as the absence of atmosphere, day/night cycle and weather, the possibility of full-disk observation at all longitudes, and the complementarity of lunar far-side observations with ground-based experiments.

The following mission statement for LUMIO was written on the basis of the previous observations [30]:

LUMIO is a CubeSat mission orbiting in the Earth–Moon region that shall observe, quantify, and characterize meteoroid impacts on the lunar far-side by detecting their impact flashes, complementing Earth-based observations of the lunar nearside, to provide global information on the lunar meteoroid environment and contribute to Lunar Situational Awareness.

The mission is divided into five main phases, represented in Figure 7.1, and better ex-

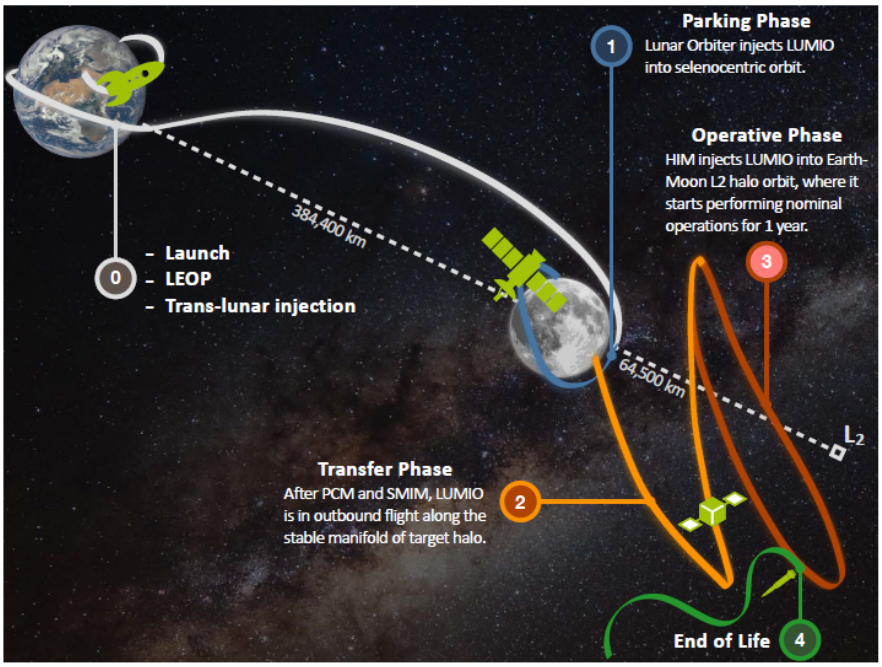

Figure 7.1: LUMIO Mission Architecture [4]

plained hereafter [31].

1. **Deployment**: which comprises the switch-on of the spacecraft, early operations, stabilization and attitude acquisition, establishment of communications, and commissioning of propulsion system.
2. **Transfer**: made by a first orbit determination, then the execution of two maneuvers: a change of plane, and a manifold injection maneuver.
3. **Commissioning**: with orbit determination and acquisition, calibration of instruments and beginning of operations.
4. **Operation**: which consists in both scientific operations, such as images acquisition and processing, and technical operations, such as communications and control maneuvers.
5. **End of Life**: with a final communication with the orbiter, and the execution of the disposal maneuver.

7.1.1. Operational Constraints

This work is centred around the operation phase of the mission. The operational orbit is chosen to be a halo orbit, about the L2 point of the Earth-Moon system. It is selected

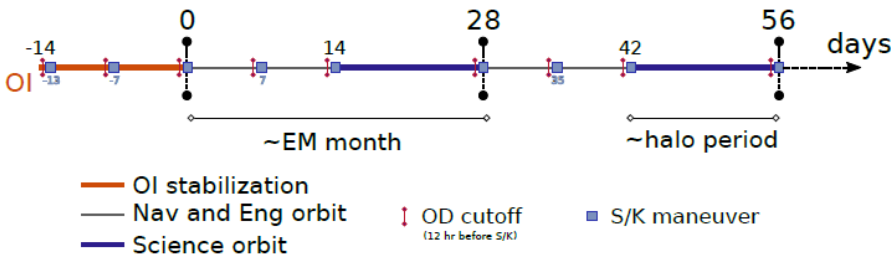

Figure 7.2: Disposition of Station-Keeping Maneuvers for LUMIO Mission [5]

through a trade-off, which includes Keplerian orbits, frozen orbits and various libration point orbits. Keplerian and frozen orbits are discarded because of their excessive fuel requirement. The halo type is selected between the libration point orbits, for its low fuel cost, both in the transfer and in the orbit maintenance [7].

The final selection of the orbit is done considering a coverage analysis, and a more detailed calculation of the fuel budget. The resulting orbit has a Jacobi constant of $C_J = 3.09$. The trajectory is generated with the method explained in Section 2.3.1, and is the one used as reference for the station-keeping simulations.

During the operation phase the orbits are divided into Science orbits, and Navigation and Engineering orbits. The placement of the orbits and, consequently, the station-keeping maneuvers, is schematized in Figure 7.2. During a Navigation and Engineering orbit the spacecraft performs three maneuvers: the first, the seventh, and the last day of the orbit. On the other hand, on Science orbits the spacecraft does not perform any maneuver. Consequently, there are intervals of 14 days without any correction to the trajectory, which is a fundamental constraint to keep in mind when designing the station-keeping strategy.

Concerning station-keeping, the two most important subsystems to consider are the propulsion system, and the attitude determination and control system. The propulsion system features one main green mono-propellant thruster, for the main maneuvers, and four cold gas RCS thrusters for de-tumbling and de-saturation.

As for the attitude determination and control system, the sensor suite is composed of a sun sensor, two star trackers and an inertial measurement unit. A set of three reaction wheels operate together with the RCS thrusters for attitude control. The orbit determination is performed using LUMIO-cam, using autonomous full-disk optical navigation.

The proprieties of those two subsystems are reflected in the values chosen for the operational errors, guaranteed by the work of Franzese et al [15]. The parameters are presented

Table 7.1: Standard Deviations of Operation Errors

Orbit Injection:	
$\sigma_x, \sigma_y, \sigma_z$	1 km, 1 km, 1 km
$\sigma_{\dot{x}}\sigma_{\dot{y}}, \sigma_{\dot{z}}$	1 cm/s, 1 cm/s, 1 cm/s
Orbit Determination:	
$\sigma_x, \sigma_y, \sigma_z$	1 km, 1 km, 1 km
$\sigma_{\dot{x}}\sigma_{\dot{y}}, \sigma_{\dot{z}}$	1 cm/s, 1 cm/s, 1 cm/s
Maneuver Execution:	
$\sigma_{\Delta\dot{x}}, \sigma_{\Delta\dot{y}}, \sigma_{\Delta\dot{z}}$	2%, 2%, 2%

in Table 7.1. Also correlated to the orbit determination process, the cutoff time is set at $t_c = 12$h.

7.2. Target Point Approach

As explained in Section 4.7, the objective of the analysis is to improve the results obtained with the parameters in Cipriano et al [5], which are reported in Table 7.2.

Table 7.2: Baseline Parameters for Target Point Approach

Parameter	Value	Unit
Δt_1	35	[d]
Δt_2	42	[d]
Q	$10^{-1} I_{3\times3}$	[∼]
R_1	$10^{-2} I_{3\times3}$	[∼]
R_2	$10^{-2} I_{3\times3}$	[∼]

A first simulation is made with the baseline parameters, and its results are reported in Table 7.3. Its fuel perfomances are worse than the ones expected in Cipriano et al. [5], because of the different approach in the implementation of orbit determination. Considering the process as a real error made by the spacecraft, instead of a displacement of the state, has a deep effect in the results and increases the mean Δv of the simulation.

The first step taken to improve the parameters is to perform a grid search over the location of the target points, with the objective of finding if the epochs of the target points are the best ones or if there is room for improvement in the selection of those parameters. The grid search is performed with a step of 1 day between the epochs, ranging between 20 and 50 days. The lower value is chosen considering the robustness of the algorithm, a target

Table 7.3: Baseline Results for Target Point Approach

Δv_{tot} [m/s/y]			Min Δv [m/s]	Max Δv [m/s]	Max Dev [km]	Fails [∼]
Ave	Range		Ave	Ave	Ave	(%)
58.17	18.23	129.82	0.016	9.62	537	0

point sooner than 20 days could cause problems in the event of a missed maneuver. The higher value, on the other hand, is selected because with target points farther in time the STM becomes ill conditioned, leading to numerical errors in the propagation and in the computation of the maneuvers. The results of the grid search are presented as a plot, in Figure 7.3.

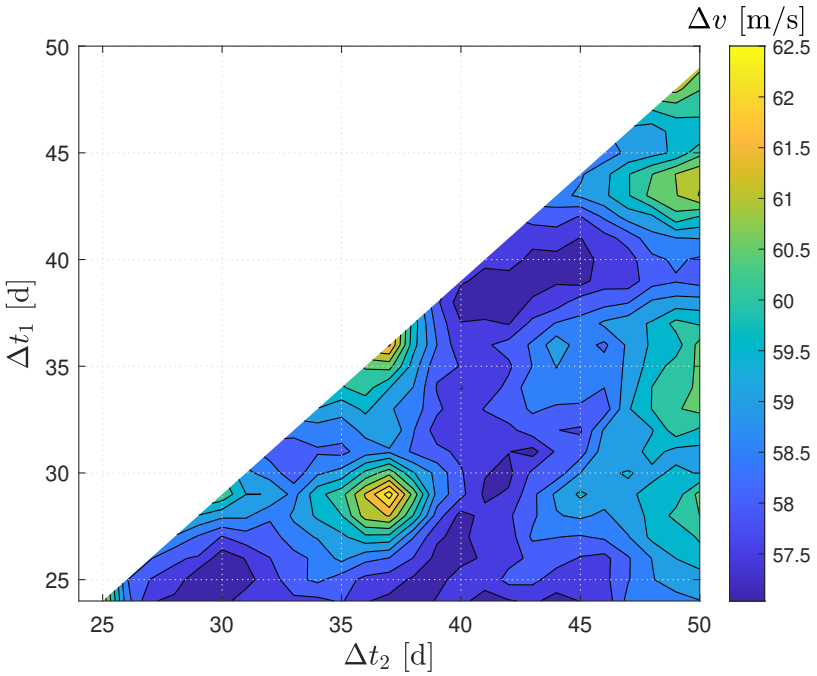

Figure 7.3: Results for Target Point Grid Search

The plot clearly shows regions in which it is unfavourable to place the target points, leading to an increase of around 10% in the fuel cost. On the other hand, there is no absolute minimum region, and there are multiple viable options for the choice of the target point epochs. The best pair found by the grid search is

$$\Delta t_1 = 23 \text{ d}, \qquad \Delta t_2 = 41 \text{ d}, \tag{7.1}$$

although the pairs $(38, 41)$ and $(25, 30)$ are also close in terms of performance. The best Δv resulting from the simulation is 56.81 m/s/y, which is a decrement of 2.3 % with respect to the baseline parameters.

The tuning of the parameters is further improved by changing the weights of the cost function. Because it is not possible to make a pork chop plot with three variables, the analysis is done by varying the coefficients one at a time. The resulting plots appear in Figure 7.4.

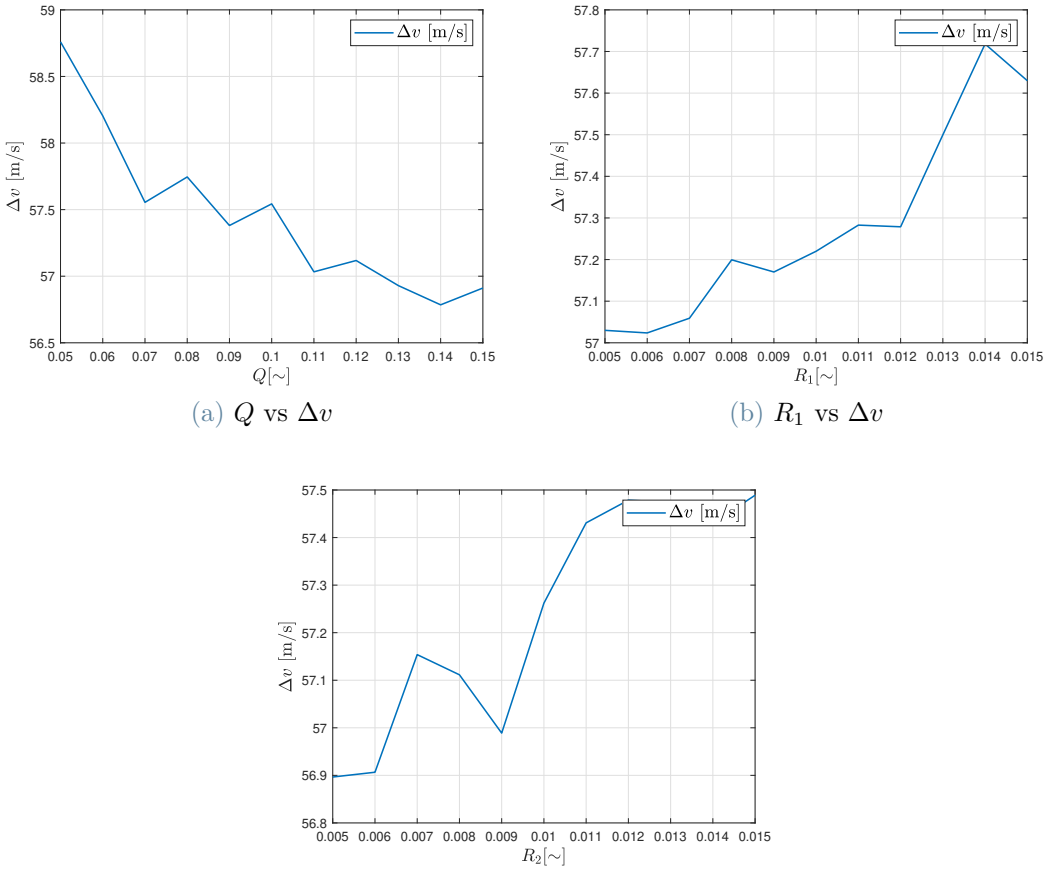

(a) Q vs Δv

(b) R_1 vs Δv

(c) R_2 vs Δv

Figure 7.4: Mean Δv as Function of TPA Weights

The plots are made in order to test the neighborhood of the baseline parameters, because those were chosen as values found to be optimal in literature. Although relatively small, the change of the weights can improve the fuel budget, especially the tuning of Q. The plots suggest that, in order to improve the performance, it is better to relax the weight of the deviation from the target points, and increase the weight of the Δv, which is a result that is intuitively correct. Following this line of reasoning, a number of simulations is done, by increasing Q and decreasing R_1 and R_2 together. The best results are found

Table 7.4: Results for Target Point Approach with Improved Weights

Δt_i [d]	Δv_{tot} [m/s/y]			Min Δv [m/s]	Max Δv [m/s]	Max Dev [km]	Fails [∼]
	Ave	Range		Ave	Ave	Ave	(%)
(23, 41)	55.92	22.03	104.13	0.01	9.49	1303	0.03
(38, 41)	56.09	19.48	109.34	0.01	9.51	1218	0
(25, 30)	55.83	20.17	113.73	0.01	9.51	1845	0.5

with values:

$$Q = 0.2, \qquad R_1 = 0.05, \qquad R_2 = 0.05. \tag{7.2}$$

After those value, a further change in the weights leads to an increase in the failed simulations, due to the maximum deviation being violated. The results obtained with the gains in Equation (7.2), and the best couples of target point epochs, are reported in Table 7.4.

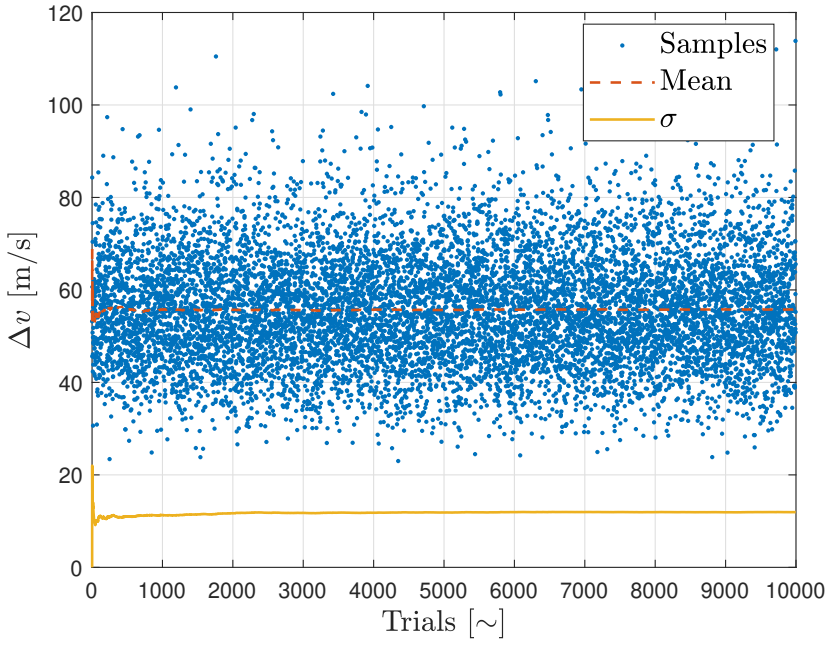

Figure 7.5: Monte Carlo Samples for Target Point Approach

The results show another, although relatively small, improvement in the Δv. In contrast, the decrement in the maximum Δv obtained by the simulations is in the order of 20% with respect to the original parameters. This makes the refined strategy more robust, requiring less fuel margin for the worst case scenario. The number of fails is still small,

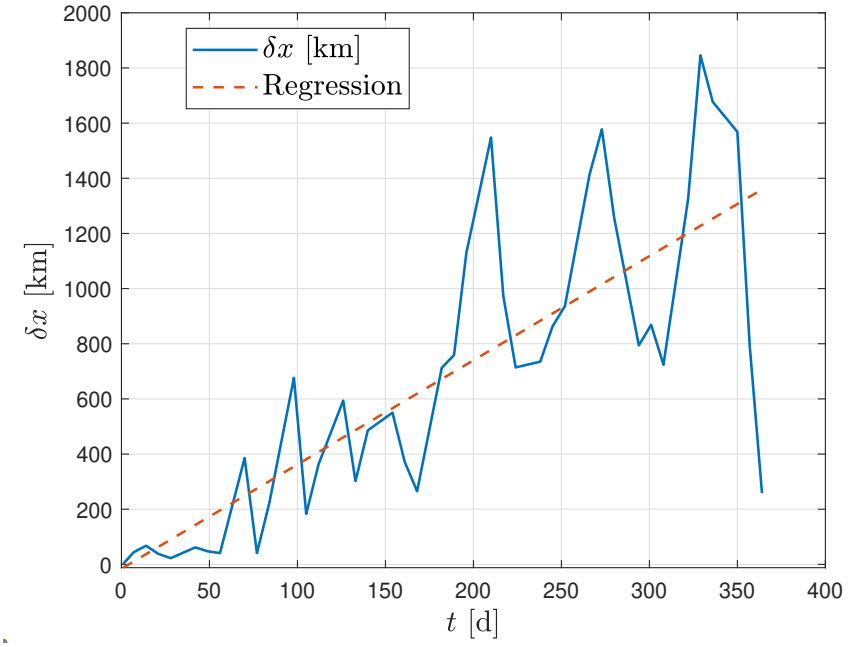

Figure 7.6: Position Deviation for Target Point Approach

although different from zero in the first and third cases, giving the results a high level of confidence. The parameter that worsens is, as expected, the maximum deviation. This is however acceptable, because the average remains well under the operational constraint.

On the basis of the previous considerations, the first result is considered as the best one, mainly because of the maximum Δv obtained in the simulation. The second option is, on the other hand, the most reliable, having scored zero fails in ten-thousands trials. The Monte Carlo samples for the final strategy are plotted in Figure 7.5. The results are statistically significant, because the mean and standard deviation have reached convergence, even before 1000 trials.

Finally, Figure 7.6 shows the position deviation over only one simulation. The results is not statistical but shows how the strategy tends to control the spacecraft. It is expected that position deviation builds up over time, and it is confirmed by the slope of the regression line. However, two things must be noted. First, most of the maneuvers prove to be successful at lowering the deviation of the spacecraft, and even though the deviation shows an increasing trend, the spacecraft remains bound to the reference trajectory. Secondly, the deviation is computed with respect to a isochronous point on the reference. This means that the position may not deviate with respect to the desired path, but only shift in time. Over the samples used for the simulations, the mean angular coefficient for the regression line is 4.47 km/d, which gives a mean final deviation of 1632 km, compat-

ible with the results. It must be noted that no cases resulted in a negative coefficient of the regression line, demonstrating that allowing some deviation to build up over time is a feature of the method.

7.3. Floquet Modes Approach

As already mentioned in Section 5.4, the goal is to test Floquet modes approach as a backup for target point approach. As foreseen by analyzing the results obtained by Gomez [17], the strategy is not able to keep the spacecraft in the vicinity of the desired trajectory. As a reference, the results of the simulations are still reported in Table 7.5. The parameters used to obtain the results are in common with target point approach, the only exception being the matrix Q from the second controller. It was defined with the values suggested by Keeter [19], which are

$$Q = \text{diag}\{1.81, 1.81, 1.15, 1.81, 1.81, 0.120, 30.1, 356\}. \tag{7.3}$$

The vast majority of the simulations are failed, because of the maximum deviation being reached. The second controller is not able to produce any successful result. With the first one, on the other hand, a small number of simulations are able to control the spacecraft. The best one even results in a Δv comparable with target point approach, but it is statistically insignificant.

The strategy is consequently tested as a backup of TPA. The algorithm is programmed such that if the unstable component α_1 is below a certain threshold value the maneuver is executed with Floquet modes approach, otherwise with TPA. This is tried with two different values of α_1, which are: $\alpha_1 = 10^{-4}$ and $\alpha_1 = 10^{-5}$. Higher values are not considered because they would lead to maneuvers which are too high in magnitude, whereas lower values are not considered because they actually never happen, and the results of the simulation would be the same as with only TPA. The outcome of those simulations

Table 7.5: Results with Floquet Mode Approach

	Δv_{tot} [m/s/y]			Min Δv [m/s]	Max Δv [m/s]	Max Dev [km]	Fails [∼]
Controller	Ave	Range		Ave	Ave	Ave	(%)
1	203.67	64.12	463.55	0.01	39.03	14958	99.5
2	N/A	N/A	N/A	N/A	N/A	N/A	100

is reported in Table 7.6.

The results clearly show that Controller 1 performs better. The first round of simulations, with $\alpha_1 = 10^{-5}$, is able to keep the average Δv close to the one of TPA. In addition, Cont. 1 has a small impact on the maximum deviation and on the success rate. In both cases the range of Δv obtained by the simulations is increased, although much more with Cont. 2. When considering $\alpha_1 = 10^{-4}$ the results worsen considerably. The ones with Cont. 2 have a number of failures that is too high to consider the strategy as viable. The ones with Cont. 1, on the other hand, have a higher success rate, but the performances are still much worse than TPA.

Another trial is made by considering the first few maneuvers done with FMA and the other with TPA. This is because the main concern for Floquet modes approach is the absence of periodicity in the orbit. It is consequently interesting to see what happens if the FMA maneuvers are applied before the perturbations given by the other planets have had time to impact the spacecraft trajectory. The results of the simulation are reported in Table 7.7.

The results show that again the second controller is not able to successfully control the spacecraft. The Δv shows an increasing trend, meaning that the FMA maneuvers are not effective. In fact, with the highest number of maneuvers done with Floquet mode approach, the simulation shows only failed attempts. The first controller, on the other hand, shows a stable trend of the Δv. To take advantage of this, the Δv is plotted against the number of maneuvers done with FMA. It is reported in Figure 7.7.

As shown in the plot, until 6 maneuvers done with FMA there are no significant changes with respect to TPA when using the first controller. After that, the fuel cost starts

Table 7.6: Results with Floquet Mode Approach as Backup to TPA

	Δv_{tot} [m/s/y]			Min Δv [m/s]	Max Δv [m/s]	Max Dev [km]	Fails [∼]
Parameters	Ave	Range		Ave	Ave	Ave	(%)
Max $\alpha_1 = 10^{-5}$							
Cont. 1	58.26	25.51	180.11	0.01	10.65	1478	0.7
Cont. 2	57.80	22.54	237.40	0.01	10.42	13168	18
Max $\alpha_1 = 10^{-4}$							
Cont. 1	75.32	21.75	257.39	0.009	18.46	3095	10
Cont. 2	77.92	28.49	213.83	0.006	19.63	76956	86

Table 7.7: Results with First Maneuvers Done with Floquet Mode Approach

	Δv_{tot} [m/s/y]			Min Δv [m/s]	Max Δv [m/s]	Max Dev [km]	Fails [∼]
Parameters	Ave	Range		Ave	Ave	Ave	(%)
First 2 Man.							
Cont. 1	56.10	17.76	118.46	0.01	9.46	1302	0
Cont. 2	58.66	21.50	112.96	0.006	9.54	1333	0.1
First 3 Man.							
Cont. 1	56.28	18.79	121.62	0.01	9.50	1296	0
Cont. 2	61.24	23.80	148.81	0.006	9.65	1315	0.1
First 4 Man.							
Cont. 1	56.12	18.52	107.00	0.01	9.49	1315	0
Cont. 2	80.53	23.25	209.88	0.006	18.42	3531	16
First 5 Man.							
Cont. 1	56.39	21.84	162.88	0.01	9.53	1308	0.05
Cont. 2	86.97	35.10	214.22	0.005	28.83	32403	84

increasing. This shows a success at blending Floquet mode and target point approach into a strategy that provides a backup to target point approach for the first few orbits. After that, probably because of the perturbations given by the solar system's planets, Floquet mode approach starts becoming disadvantageous to use.

As shown for target point approach, the Monte Carlo trials are plotted in Figure 7.8. The specific plot was made considering the first four maneuvers done with FMA. It is demonstrated that 10000 trials are enough to produce statistically significant results. In fact, the standard deviation reaches convergence well before 1000 trials.

Finally, the position deviation for the hybrid strategy, performed with controller 1, is plotted in Figure 7.9. The rise of the deviation in the first maneuvers is faster than with target point, given the minor effectiveness of Floquet mode approach for the reference orbit. The number of maneuver performed with FMA, however, is small enough to allow TPA to stabilize the spacecraft afterwards. In fact, the plot looks similar to the one of Target point approach after the first maneuvers. This is additionally confirmed by the fact that the number of failures detected with the hybrid strategy is as small as with TPA alone. The mean inclination of the regression line is 5.37 km/d, higher than with TPA alone, and confirmed by the higher mean final deviation seen in Tables 7.6 and 7.7.

The last simulation is performed to validate the previous results. The validation is done

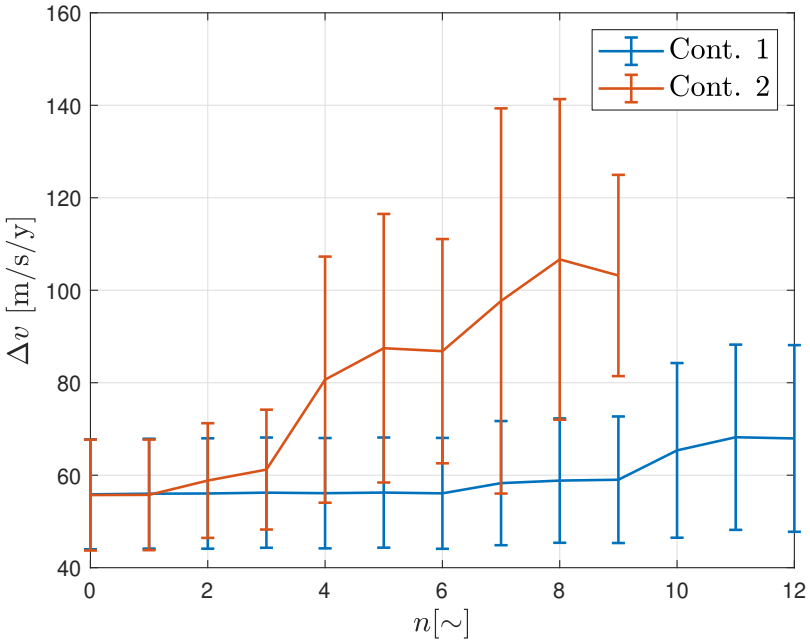

Figure 7.7: Mean Δv as Function of the Number of FMA Maneuvers

against the results obtained by Gomez et al [17]. The reference orbit considered has a Jacobi constant of $C_J = 3.16$, and belongs the family of halos considered in the design of LUMIO. It is not exactly the orbit used in the reference, but it is the closest one available in the halo family generated for LUMIO. The frequency of the maneuvers is changed to one every two days, and the other parameters are left as in the previous analysis. The results of the validation are reported in Table 7.8.

The results are similar to each other, although not equal. The first cause could be that they are obtained with Monte Carlo simulations, which never produces exactly the same results. To be more specific, Gomez introduces other filters into the simulation. There are several tracking interval, and a maneuver is performed only if an exponential increase in α_1 is detected in three consecutive trackings. There is also a condition for which a

Table 7.8: Validation Against Gomez et al. Results

	Δv_{tot} [m/s/y]			Min Δv [m/s]	Max Δv [m/s]	Max Dev [km]	Fails [$\sim$]
Results	Ave	Range		Ave	Ave	Ave	(%)
LUMIO	6.61	4.97	8.84	0.0003	0.15	111	0
Gomez et al.	6.21	5.17	11.01	0.03	0.21	N/A	N/A

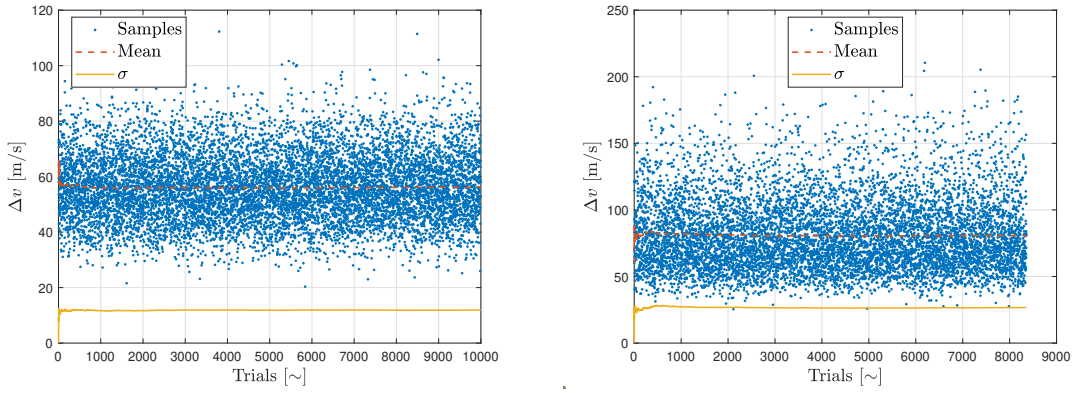

(a) Controller 1 (b) Controller 2

Figure 7.8: Monte Carlo Samples of Floquet Mode Approach

maneuver is not performed if it has a magnitude lower than a threshold value. Those two additional conditions cause different results, and produce a much higher change than the sole randomness of the operational errors.

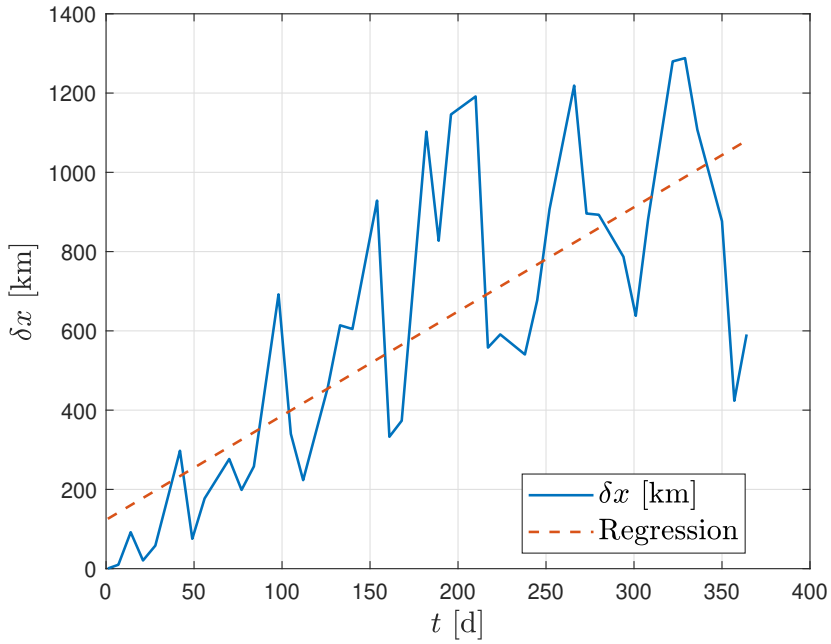

Figure 7.9: Position Deviation of Hybrid Strategy with Controller 1

In conclusion, the results obtained with the analysis done with Floquet mode approach are considered valid, thanks to the comparison with the work of Gomez et al [17]. Although the strategy is not able to successfully control the spacecraft, it is demonstrated that a blend between FMA and TPA is possible. Floquet mode approach is advantageous in

the first stages of the mission, when the motion has not been perturbed yet by the other solar system planets, whereas target point approach is more suitable to counteract those forces. The final hybrid strategy leads to results which are interchangeable with target point approach.

7.4. Short Term Approach

Short term approach is implemented to test its performance on the case study of LUMIO. For this work two different strategies are investigated:

1. Strategy 1 involves the targetting of the next maneuver point. This means that the target point is either 7 or 14 days after the maneuver.
2. Strategy 2, on the other hand, always targets a point 14 days after the maneuver, to provide a maneuver that continues the trajectory for one orbit.

The selection of a target point farther in time is prevented by the use of the simple-shooting method. Either a multiple-shooting scheme or additional conditions would be necessary to continue the orbit for additional time.

The main difficulty encountered with the implementation is the high computational cost. For this reason, the number of simulations for the Monte Carlo analysis is set to 100. The investigation is performed on a Windows PC, equipped with a Intel Core i7 7700k processor, with a base frequency of 4.20 GHz, and with all four cores running in parallel. Computing 100 trials of Strategy 2 takes more than 1 day, with Strategy 1 being slightly less computationally heavy, because of the shorter time span of the simple-shooting method.

The results obtained with both strategies, using the short term approach, are reported in Table 7.9. The first results that stand out are the mean maximum deviation and the number of failures. These however have to be associated with the simple shooting method converging to solutions that are feasible but very far from the reference trajectory. These cases can be graphically seen when doing the simulation, and may be avoided by improving

Table 7.9: Results of Short Term Approach

	Δv_{tot} [m/s/y]			Min Δv [m/s]	Max Δv [m/s]	Max Dev [km]	Fails [∼]
Results	Ave	Range		Ave	Ave	Ave	(%)
Strat. 1	105.78	39.14	201.39	0.03	14.37	13915	62
Strat. 2	79.64	38.57	155.21	0.03	10.12	54997	69

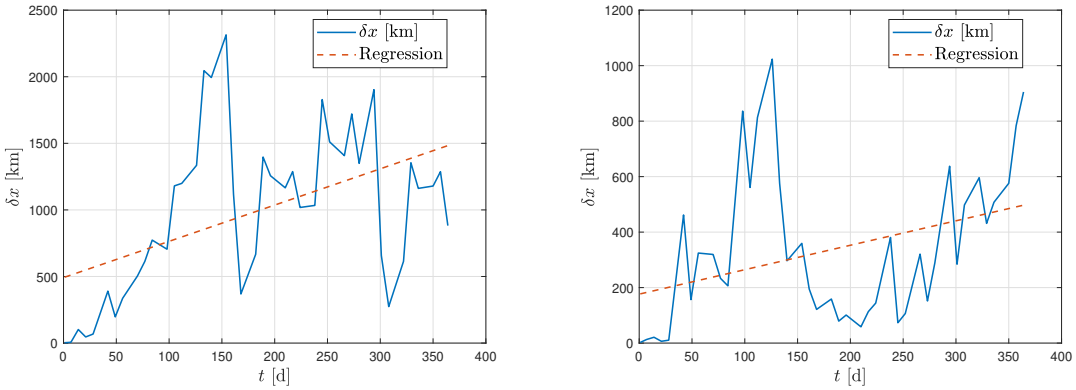

(a) Strategy 1 (b) Strategy 2

Figure 7.10: Position Deviation of Short Term Approach

the initial guess of the simple-shooting, for example with a differential correction scheme, or by adding additional constraints to the method. When considering only the successful cases, the mean deviation is in the order of hundreds of km, which is much lower than target point approach. Even though additional work has to be done to consider the method safe, it must be pointed out that the successful cases show that this strategy can reliably maintain the spacecraft near the reference trajectory. This is supported also by Figure 7.10. It can be noticed that the curve for Strategy 1 resembles in some way the one for TPA, whereas Strategy 2 performs better than all the other strategies. The values on the y axis are much smaller, and the regression line is more shallow than the others. Short term approach, consequently, seems like a viable strategy if the deviation is a constraint for the mission, although the problems with the convergence of the simple shooting have to be addressed.

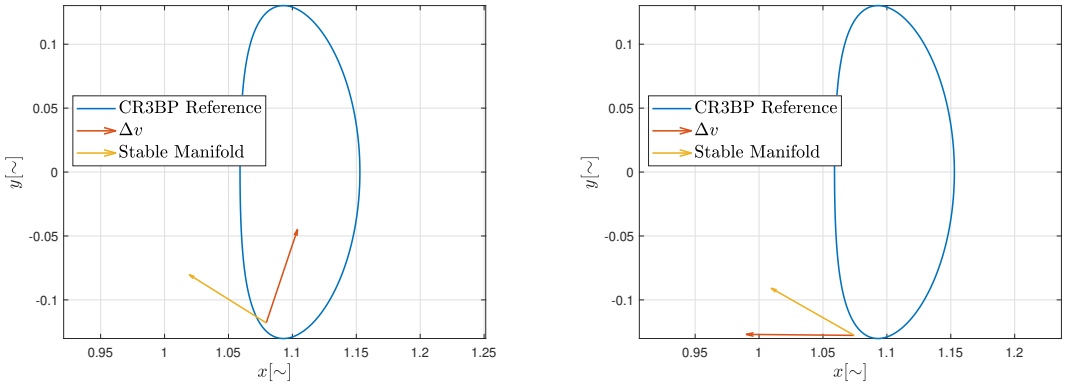

(a) Strategy 1 (b) Strategy 2

Figure 7.11: Alignment Between Δv and Stable Manifold

Regarding the different strategies, Strategy 2 results in a much lower fuel cost, but fails more frequently. It is interesting to see that performing a simple-shooting that has a target point farther in time gives better performance. The strategy may give better results, hopefully better than target point, if implemented with a target point two or three orbits in advance. It is however impossible to compute such a maneuver with the simple-shooting explained in Chapter 6. The method should be improved either with a multiple-shooting method or with additional constraints.

An important feature of the short term approach, discussed in the work of Pavlak and Howell [26], is the fact that maneuvers, even though computed with a gradient based solver, tend to align with the stable manifold. This fact is analyzed in Figure 7.11. It can be seen that the alignment is present for Strategy 2, whereas in Strategy 1 the two vectors are almost perpendicular. This could be a hint of the better fuel performance of Strategy 2. What is interesting to notice, is that the Δv of Strategy 1 tends to be opposite with respect to the unstable manifold, as shown in Figure 7.12. This feature is not presented in the work by Pavlak and Howell, but seems to be consistent for the entire station-keeping simulation. Although the plots present a single maneuver, this facts are checked for multiple maneuvers in various simulations, and are in accordance with the inspections performed.

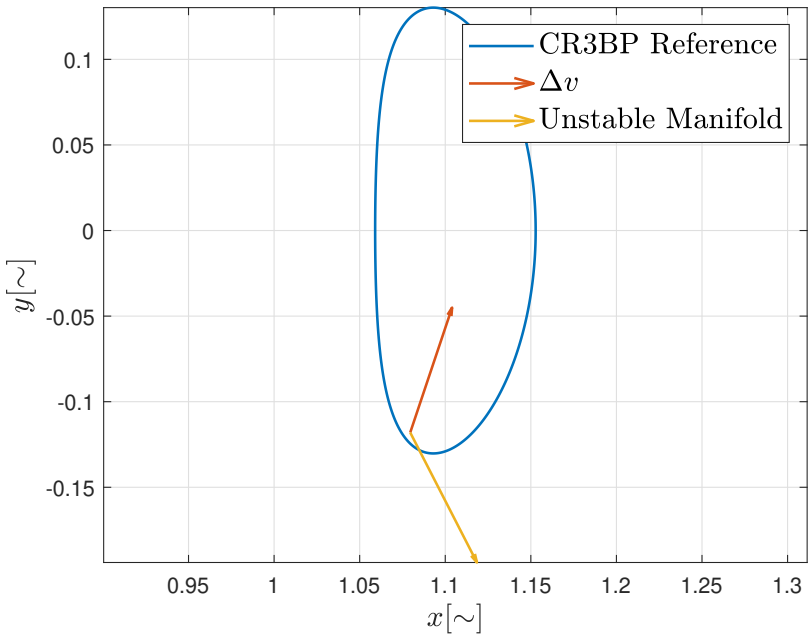

Figure 7.12: Alignment Between Δv and Unstable Manifold

To finally validate the results, it must be noted that, for both strategies, the mean result is obtained with more than 30 valid simulations, which the lower theoretical limit to

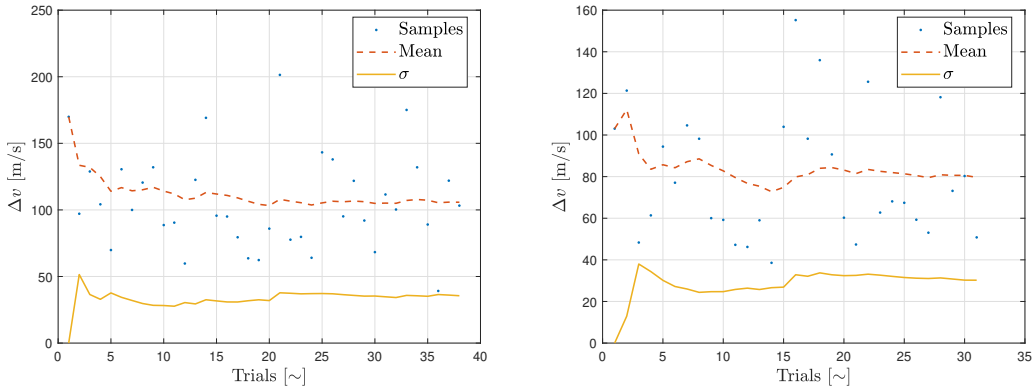

(a) Strategy 1 (b) Strategy 2

Figure 7.13: Monte Carlo Samples with Short Term Approach

use normal distributions for the operational errors. The samples of the Monte Carlo simulations are plotted, for both strategies, in Figure 7.13. Although some oscillations are still present in the mean, the standard deviation has reached sufficient convergence, and those oscillations would change the results by an amount lower than 5%. The results are thus considered valid.

8 | Conclusions

The primary goal of this research is the investigation of the station-keeping problem, applied to the case study of LUMIO mission. To achieve this objective, the equations of motion are first derived, both in the circular restricted hypothesis and in the high fidelity roto-pulsating model, that is the one used to obtain the final results. After that, some existent station-keeping strategies are reviewed, in order to make a trade-off and select which ones to implement. This work focuses on Floquet mode approach and short term approach. Considering that target point approach is the baseline technique for the mission, some effort is also spent to improve the tuning of the parameters of TPA.

The station-keeping strategies are then implemented inside a simulation algorithm that models the real mission scenario, with operational errors. The code is ran multiple times to conduct a Monte Carlo analysis, in order to gather statistically significant data. The results show that target point approach can be slightly improved by changing the parameters. Short term approach, on the other hand, is not successful at improving the average Δv. Finally, Floquet mode approach, while being unable to control the spacecraft by itself, is able, when blended with TPA, to serve as a backup strategy for the first few orbits, without significantly changing the performances of TPA. The results are finally compared with an authoritative literature source, to test their validity.

To finally answer the research question, even though this work is unable to massively reduce the fuel cost for the station-keeping of LUMIO, it shows that the reliability can be improved by implementing Floquet mode approach as backup strategy for the first maneuvers of the mission. The mission can now consider a second option in case of any problem with target point approach, but only for the first two orbits.

8.1. Future Developments

Regarding the possible future improvements of this work, two different areas can be addressed: one related to the station-keeping of libration point orbits, and the other specific to LUMIO mission.

For what concerns libration point orbits, target point approach has been deeply investigated by various researchers, and there is plenty of literature material available. Floquet mode approach seems like a very promising method when applied in the CR3BP, but its performance degrades when implemented in the RPRnBP. There is consequently a necessity of improving the mathematical framework related to Floquet modes, by either extending it to quasi-periodic orbits, or testing whether it is a viable strategy for simulations in higher fidelity models. Regarding the short term approach, it was mainly tested in the design of ARTEMIS mission. It would be fruitful to extend the investigation to other kinds of libration point orbits. In general, the research about station-keeping, as seen in the first Chapter, seems to be focused mainly on halo and Lissajous trajectories. The analysis of other kinds of orbits, such as Lyapunov orbits, can be of practical interest for future works.

As for LUMIO mission, target point approach has been investigated multiple times, leading to an improvement thanks to the tuning of the parameter. A possibility not yet analyzed is time varying weight matrices, which could lead to a further improvement of the fuel budget. Floquet mode approach is shown to be evanescent at controlling the spacecraft on the orbit of LUMIO. However, with an orbit with higher Jacobi constant, it can be better than target point approach, due to the orbits being more quasi-periodic. Short term approach has turn out to be more expansive than target point approach. However, it could be improved in two ways. One is the implementation of the multiple shooting method, to allow the target point to be farther in time. The other is the investigation of the orbit continuation strategy, where the target point is substituted by user defined constraints, and there is no need for a reference trajectory. The definition of the constraints is of interest, because they are only found in literature for the ARTEMIS mission, and are not available for halo orbits.

The interest in libration point missions will continue to grow in the future due to the unique configuration that they provide. The feasibility and success of those missions are inextricably linked to the development of station-keeping strategies, and this work is presented in the hope that the investigations conducted will contribute to the success of LUMIO, and other future libration point missions.

Bibliography

[1] X. Bai and J. L. Junkins. Modified chebyshev-picard iteration methods for solution of boundary value problems. *The Journal of the astronautical sciences*, 58(4):615–642, 2011. doi: https://doi.org/10.1007/BF03321534.

[2] X. Bai and J. L. Junkins. Modified chebyshev-picard iteration methods for station-keeping of translunar halo orbits. *Mathematical Problems in Engineering*, 2012, 2012. doi: https://doi.org/10.1155/2012/926158.

[3] J. V. Breakwell, A. A. Kamel, and M. J. Ratner. Station-keeping for a translunar communication station. *Celestial Mechanics*, 10(3):357–373, 1974.

[4] A. Cervone, F. Topputo, S. Speretta, A. Menicucci, E. Turan, P. Di Lizia, M. Massari, V. Franzese, C. Giordano, G. Merisio, D. Labate, G. Pilato, E. Costa, E. Bertels, A. Thorvaldsen, A. Kukharenka, J. Vennekens, and R. Walker. LUMIO: A CubeSat for observing and characterizing micro-meteoroid impacts on the Lunar far side. *Acta Astronautica*, 195:309–317, 2022. ISSN 0094-5765. doi: https://doi.org/10.1016/j.actaastro.2022.03.032.

[5] A. M. Cipriano, D. A. Dei Tos, and F. Topputo. Orbit Design for LUMIO: The Lunar Meteoroid Impacts Observer. *Frontiers in Astronomy and Space Sciences*, 5, 2018. ISSN 2296-987X. doi: 10.3389/fspas.2018.00029.

[6] S. Cravedi. Orbit maintenance strategy for libration point orbits, floquet modes approach. Master's thesis, Politecnico di Milano, 2019.

[7] D. A. Dei Tos. *Trajectory optimization of limited control authority spacecraft in high-fidelity models*. PhD thesis, Politecnico di Milano, 2018.

[8] D. A. Dei Tos and F. Topputo. Trajectory refinement of three-body orbits in the real solar system model. *Advances in Space Research*, 59(8):2117–2132, 2017. ISSN 0273-1177. doi: https://doi.org/10.1016/j.asr.2017.01.039.

[9] D. A. Dei Tos and F. Topputo. High-fidelity trajectory optimization with application

to saddle-point transfers. *Journal of Guidance, Control, and Dynamics*, 42(6):1343–1352, 2019. doi: 10.2514/1.G003838.

[10] E. J. Doedel, V. A. Romanov, R. C. Paffenroth, H. B. Keller, D. J. Dichmann, J. Galán-vioque, and A. Vanderbahuwede. Elemental periodic orbits associated with the libration points in the circular restricted 3-body problem. *International Journal of Bifurcation and Chaos*, 17(08):2625–2677, 2007. doi: 10.1142/S0218127407018671.

[11] R. W. Farquhar. Lunar communications with libration-point satellites. *Journal of Spacecraft and Rockets*, 4(10):1383–1384, 1967. doi: 10.2514/3.29095.

[12] R. W. Farquhar. The flight of isee-3/ice: origins, mission history, and a legacy. *The Journal of the astronautical sciences*, 49(1):23–73, 2001.

[13] D. Folta, T. Pavlak, K. Howell, M. Woodard, and D. Woodfork. Stationkeeping of lissajous trajectories in the earth-moon system with applications to artemis. In *AAS/AIAA Space Flight Mechanics Meeting*, number 1055 in LEGNEW-OLDGSFC-GSFC-LN, 2010.

[14] D. Folta, M. Woodard, and D. Cosgrove. Stationkeeping of the first earth-moon libration orbiters: the artemis mission. In *AAS/AIAA Astrodynamics Specialist Conference*, number 2011 in GSFC. CP. 4858., 2011.

[15] V. Franzese, P. Di Lizia, and F. Topputo. Autonomous optical navigation for lumio mission. In *2018 Space Flight Mechanics Meeting*, 01 2018. doi: 10.2514/6.2018-1977.

[16] G. Gómez, J. Llibre, R. Martınez, and C. Simó. Station keeping of a quasiperiodic halo orbit using invariant manifolds. In *Proceed. 2nd Internat. Symp. on spacecraft flight dynamics, Darmstadt*, pages 65–70, 1986.

[17] G. Gómez, K. Howell, J. Masdemont, and C. Simó. Station-keeping strategies for translunar libration point orbits. *Advances in Astronautical Sciences*, 99(2):949–967, 1998.

[18] G. Gòmez, J. Masdemont, and J. Mondelo. *Dynamical substitutes of the libration points for simplified solar system models*, pages 373–397. World Scientific, 2003. doi: 10.1142/9789812704849_0017.

[19] K. C. Howell and T. M. Keeter. Station-keeping strategies for libration point orbits-target point and floquet mode approaches. *Spaceflight mechanics 1995*, pages 1377–1396, 1995.

[20] K. C. Howell and H. J. Pernicka. Station-keeping method for libration point tra-

jectories. *Journal of Guidance, Control, and Dynamics*, 16(1):151–159, 1993. doi: 10.2514/3.11440.

[21] Y. Lian, G. Gómez, J. J. Masdemont, and G. Tang. Station-keeping of real earth–moon libration point orbits using discrete-time sliding mode control. *Communications in Nonlinear Science and Numerical Simulation*, 19(10):3792–3807, 2014. ISSN 1007-5704. doi: https://doi.org/10.1016/j.cnsns.2014.03.026.

[22] M. Lo, K. Williams, R. Wilson, K. Howell, and B. Barden. Genesis Halo Orbit Station Keeping Design. In *Spaceflight Dynamics Biarritz, France*. Root, 2000. doi: 2014/15031.

[23] A. P. Markeev. *Libration points in celestial mechanics and cosmic dynamics.* Izdatel'stvo Nauka, 1978.

[24] J. Moser. On the generalization of a theorem of a. liapounoff. *Communications on Pure and Applied Mathematics*, 11(2):257–271, 1958. doi: https://doi.org/10.1002/cpa.3160110208.

[25] T. Pavlak and K. Howell. Strategy for optimal, long-term stationkeeping of libration point orbits in the earth-moon system. In *AIAA/AAS Astrodynamics Specialist Conference*, page 4665, 2012. doi: 10.2514/6.2012-4665.

[26] T. Pavlak and K. C. Howell. Strategy for long-term libration point orbit stationkeeping in the earth-moon system. In *Proceedings of the AAS/AIAA Astrodynamics Specialist Conference, AAS Paper*, number 516 in 11, 2011.

[27] T. A. Pavlak. *Trajectory design and orbit maintenance strategies in multi-body dynamical regimes*. PhD thesis, Purdue University, 2013.

[28] M. Shirobokov, S. Trofimov, and M. Ovchinnikov. Survey of station-keeping techniques for libration point orbits. *Journal of Guidance, Control, and Dynamics*, 40 (5):1085–1105, 2017. doi: 10.2514/1.G001850.

[29] V. Szebehely. *Theory of orbit: The restricted problem of three Bodies*. Elsevier, 2012.

[30] F. Topputo, M. Massari, J. Biggs, P. Di Lizia, D. Dei Tos, K. Mani, S. Ceccherini, V. Franzese, A. Cervone, and e. a. Sundaramoorthy, P. Lunar Cubesats for Exploration. Lumio: Lunar Meteoroid Impacts Observer, 2017.

[31] F. Topputo, M. Massari, J. Biggs, P. Di Lizia, D. Dei Tos, K. Mani, S. Ceccherini, V. Franzese, A. Cervone, P. Sundaramoorthy, et al. Lumio: a cubesat at earth-moon l2. In *4S Symposium*, pages 1–15, 2018.

[32] D. A. D. Tos and N. Baresi. *Genetic optimization for the orbit maintenance of libration point orbits with applications to EQUULEUS and LUMIO*, page 466. 2020. doi: 10.2514/6.2020-0466.

[33] T. Villela, C. A. Costa, A. M. Brandão, F. T. Bueno, and R. Leonardi. Towards the thousandth CubeSat: A statistical overview. *International Journal of Aerospace Engineering*, 2019, 2019. doi: https://doi.org/10.1155/2019/5063145.

[34] W. Wiesel and W. Shelton. Modal control of an unstable periodic orbit. *Journal of the Astronautical Sciences*, 31(1):63–76, 1983.

[35] W. E. Wiesel and D. J. Pohlen. Canonical floquet theory. *Celestial Mechanics and Dynamical Astronomy*, 58(1):81–96, 1994.

List of Figures

List of Tables

List of Symbols

Variable	Description	SI unit
a	Orbital Radius of First Primary	[km]
$\boldsymbol{a}_{SRP}$	Acceleration due to Solar Radiation Pressure	[km/s^2]
b	Orbital Radius of Second Primary	[km]
$\boldsymbol{b}$	Transaltion of Origin from SSBF to RPF	[km]
C	Rotation Matrix from SSBF to RPF	[$\sim$]
C_J	Jacobi Constant	[$\sim$]
$\boldsymbol{d}_i$	Distance to i-th Target Point	[$\sim$]
$\tilde{E}$	Floquet Modes	[$\sim$]
$\boldsymbol{F}$	Gravitational Force Vector	[N]
$\boldsymbol{f}$	Right Hand Side of Equations of Motion	[$\sim$]
G	Universal Constant of Gravity	[N m^2 / kg^2]
I	Identity Matrix	[$\sim$]
J	Cost Function	[$\sim$]
$\tilde{J}$	Matrix of Poincarè Exponents	[$\sim$]
k	Scaling Factor of RPF	[km]
L_i	i-th Lagrangian Point	[$\sim$]
M	Monodromy Matrix	[$\sim$]
m	Mass	[kg]
Q	Weight Matrix	[$\sim$]
R_i	Weight Matrix of i-th Target Point	[$\sim$]
r	Position Vector	[km, $\sim$]
S	Matrix of Eigenvectors	[$\sim$]
T	Kinetic Energy	[km^2/s^2]
t	Time	[s]
t_c	Cutoff Time	[h]
t_i	i-th Target Point Epoch	[d]
t_v	Maneuver Epoch	[d]
V	Potential Energy	[km/s^3]

$\boldsymbol{x}$	Adimensional State Vector	[∼]
α_1	Unstable Component of Motion	[∼]
Δv_{tot}	Average Station-Keeping Cost	[m/s/y]
$\delta\boldsymbol{x}$	Perturbed State Vector	[∼]
Φ	State Transition Matrix	[∼]
$\boldsymbol{\varphi}$	Flow of Equations of Motion	[∼]
λ_i	i-th Eigenvalue of Monodromy Matrix	[∼]
μ	Adimensional Gravity Constant	[∼]
Ω	Pseudo Potential	[∼]
ω	Angular Velocity	[rad/s]
ω_i	i-th Poincarè Exponent	[∼]
$\boldsymbol{\pi}$	Vector of Projection Factors	[∼]
$\boldsymbol{\rho}$	Adimensional Position in Synodic Frame	[∼]
$\hat{\boldsymbol{\rho}}$	Position in Synodic Frame	[km]
σ	Standard Deviation	[∼]
τ	Adimensional Time	[∼]

List of Acronyms

Acronym	Definition
CR3BP	Circular Restricted Three-Body Problem
FMA	Floquet Mode Approach
LPO	Libration Point Orbit
LTA	Long Term Approach
LUMIO	Lunar Meteoroid Impact Observer
MCPI	Modified Chebishev-Picard Iterations
RPF	Roto-Pulsating Frame
RPRnBP	Roto-Pulsating Restricted n-Body Problem
SMC	Sliding Mode Control
SSBF	Solar System Baricentric Frame
STA	Short Term Approach
STM	State Transition Matrix
TPA	Target Point Approach

Acknowledgements

Vorrei innanzitutto ringraziare il Prof. Francesco Topputo, per avere accettato di seguirmi, in qualità di supervisore, lungo questo periodo di tesi, e per i suoi insegnamenti, anche durante i corsi. Ringrazio inoltre Carmine Giordano e Carmine Buonagura, per i consigli durante questa avventura.

Ringrazio poi gli amici, sia quelli di sempre, di Vigevano, del mare o della montagna, che quelli nuovi dell'università. Parte di questo traguardo lo devo a voi, sia per i momenti di crescita, sia per quelli più leggeri, di grande divertimento e delirio.

Un affettuoso ringraziamento anche a Tiziana, che mi ha tenuto compagnia durante tutto il percorso universitario, ed ha dovuto sopportare tutte le complessità che derivano da una mente sempre più ingegneristica.

Infine, il ringraziamento va alla mia famiglia, mamma Stefania e papà Roberto, e mia sorella Cecilia. Il successo in questo percorso universitario è dovuto principalmente al modo in cui sono stato cresciuto, e ve ne sono grato. Il ringraziamento è esteso, ovviamente, anche ai nonni, gli zii, sia di sangue che acquisiti, e i cugini, che sono sempre parte della famiglia.

Filippo Zanellati